

AD-A046 632

ILLINOIS UNIV AT CHICAGO CIRCLE DEPT OF PHYSICS

F/G 20/3

MAGNETISM IN TRANSITION-GROUP ALLOYS AND RARE-EARTH COMPOUNDS. (U)

SEP 77 J S KOUVEL

N00014-75-C-0895

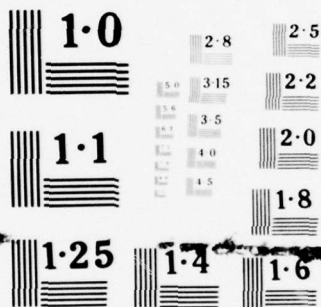
NL

UNCLASSIFIED

1 OF 1
ADA
046632



END
DATE
FILMED
12-77
DDC



NATIONAL BUREAU OF STANDARDS
MICROCOPY RESOLUTION TEST CHART

AD A 0 4 6 6 3 2

12

B.S.

MAGNETISM IN TRANSITION-GROUP ALLOYS
AND RARE-EARTH COMPOUNDS

James S. Kouvel
Department of Physics
University of Illinois at Chicago Circle
Chicago, Illinois 60680

FINAL TECHNICAL REPORT

on research conducted during the period
1 April 1974 to 30 June 1976
with the support of grants from the
Office of Naval Research

Controlling Office:
ONR Electronic and Solid
State Sciences Program
Arlington, VA 22217

Monitoring Office
ONR Branch Office
536 S. Clark Street
Chicago, IL 60605

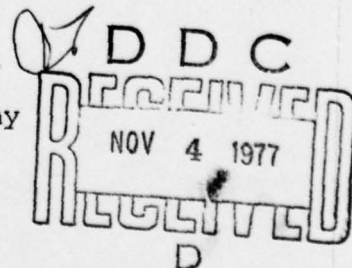
Report No. NR318-031-F

September 1977

DDC FILE COPY

Approved for public release; distribution unlimited.

Reproduction in whole or in part is permitted for any
purpose of the United States Government.



ACCESSION FOR	
NTIS	White Section <input checked="" type="checkbox"/>
DDC	Full Section <input type="checkbox"/>
UNANNOUNCED	<input type="checkbox"/>
JUSTIFICATION	
BY	
DISTRIBUTION/AVAILABILITY CODES	
Dist.	AVAIL. and/or SPECIAL
A	

(6) **MAGNETISM IN TRANSITION-GROUP ALLOYS
AND RARE-EARTH COMPOUNDS.**

(10) **James S. Kouvel**
Department of Physics
University of Illinois at Chicago Circle
Chicago, Illinois 60680

(9) **FINAL TECHNICAL REPORT.**
on research conducted during the period
1 April 1974 ~~to~~ 30 June 1976
with the support of grants from the
Office of Naval Research

(15) **NO0014-75-C-0895,
NO0014-69-A-0070-PPP3**

Controlling Office:
ONR Electronic and Solid
State Sciences Program
Arlington, VA 22217

Monitoring Office
ONR Branch Office
536 S. Clark Street
Chicago, IL 60605

Report No. NR318-031-F

(11) **September 1977**

(12) **53p.**

Approved for public release; distribution unlimited.

Reproduction in whole or in part is permitted for any
purpose of the United States Government.

**DDC
RECEIVED
NOV 4 1977
RECEIVED**

3/10 1473
392775

LB

MAGNETISM IN TRANSITION-GROUP ALLOYS
AND RARE-EARTH COMPOUNDS

James S. Kouvel
Department of Physics
University of Illinois at Chicago Circle
Chicago, Illinois 60680

ABSTRACT

Magnetization measurements were carried out in a study of local magnetic effects (magnetic clusters, paramagnons, etc.) in the transition-group alloy systems, Ni-Rh, Pd-Ni, and Fe-Cr, near their critical compositions or critical temperatures for ferromagnetic ordering. Similar measurements were made of the detailed magnetization processes associated with the micro-magnetic (spin-glass) ordering of Cu-Mn alloys. Also conducted was a magnetic and neutron diffraction investigation of high-order (biquadratic) exchange interactions in the rare-earth compounds, PrAg and DySb.

TABLE OF CONTENTS

	Page
Introduction.....	1
Experimental Results and Discussion.....	4
References.....	11
Appendix A: "Magnetic Properties of Ni-Rh Alloys..... Near the Critical Composition for Ferromagnetism" by W. C. Muellner and J. S. Kouvel (Phys. Rev. B <u>11</u> , 4552, 1975).	14
Appendix B: "Giant Moments in Paramagnetic Pd-Ni..... Alloys" by D. Sain and J. S. Kouvel (Abstract, APS March Meeting, 1976).	22
Appendix C: "Critical Magnetic Properties of..... Fe-Cr Alloys" by A. T. Aldred and J. S. Kouvel (Physica <u>86-88B</u> , 329, 1977).	23
Appendix D: "The Mictomagnetic Transition in..... Cu-Mn" by H. Claus and J. S. Kouvel (Solid State Commun. <u>17</u> , 1553, 1975).	26
Appendix E: "Biquadratic Exchange Coupling and..... the Magnetic Properties of PrAg" by T. O. Brun, J. S. Kouvel, and G. H. Lander (Phys. Rev. B <u>13</u> , 5007, 1976).	29
Appendix F: "Field-Induced Transitions in DySb"..... by T. O. Brun, G. H. Lander, F. W. Korty and J. S. Kouvel (AIP Conf. Proc. <u>24</u> , 244, 1975).	43
Appendix G: "Biquadratic Exchange Interactions..... in Rare-Earth Compounds" by J. S. Kouvel, T. O. Brun, and F. W. Korty (Physica <u>86-88B</u> , 1043, 1977).	45
Report Documentation Page (DD Form 1473).....	48
Distribution List.....	50

INTRODUCTION

The magnetism of alloys containing metals of the first transition group (the iron group) is a major unresolved area of solid state physics in which there is considerable current interest. Although definitive advances have been made towards an understanding of isolated magnetic impurity atoms in a metallic host, the more complex problem concerning the magnetic states of concentrated, atomically disordered alloys continues to pose important basic questions. Some of these questions, however, appear to be answered by the recent discoveries of intrinsically inhomogeneous magnetic states in certain concentrated nickel-based alloys (specifically, Ni-Cu¹⁻⁵ Ni-V,^{6,7} and Ni-Rh⁸⁻¹⁰). A new phenomenological picture has emerged for the magnetism of these alloys, in which the formation and size of a stable magnetic moment of a transition-group atom are critically determined by the local environment.¹¹⁻¹⁴ The broad statistical distribution of local environments in these solid-solution alloys gives rise to ferromagnetic and paramagnetic states that are spatially inhomogeneous. However, much remains to be learned about the various local conditions for stable or nearly stable magnetic moments in different systems.

In a related class of transition-group alloys known as spin glasses or mictomagnets,¹⁵ the ordered magnetic state is also thought to be spatially inhomogeneous. However, the inhomogeneity in this case refers mainly to the directions rather than the magnitudes of the moments of the randomly situated magnetic atoms. This orientational inhomogeneity is considered to arise from an

oscillation in the sign of the exchange coupling, between ferromagnetic and antiferromagnetic, as a function of distance. For the prototypal spin-glass systems, Cu-Mn and Au-Fe, it has recently been observed^{16,17} that the very pronounced irreversibilities in their magnetic properties (known from earlier work)^{18,19} set in precisely at the so-called freezing temperature, which is marked by a sharp peak in the initial susceptibility²⁰ and depends on the alloy composition. The irreversibility of the magnetization with field and temperature has been tentatively attributed to some type of local magnetic anisotropy,^{18,21,22} but the underlying microscopic mechanism is still unknown. At present, there are conflicting opinions even about the nature of the mictomagnetic (ferro-antiferromagnetic) ordering or freezing process. Thus, many of the basic questions about the magnetism of these alloys remain unresolved.

With regard to transition-group alloys, our research program involved detailed experimental studies of the thermodynamic properties of Ni-Rh, Pd-Ni, Fe-Cr, and Cu-Mn alloys near their critical compositions or temperatures for the onset of ferromagnetic or mictomagnetic order. The summary purpose of these investigations was the determination of the essential inhomogeneous character of the ordered magnetic states and the paramagnetic states from which they derive in concentrated solid-solution alloys.

The magnetism of rare-earth metals and intermetallic compounds, compared to that of their transition-group counterparts, is quite

well understood. Almost without exception, the magnetic moments of rare-earth atoms in a metal derive from well-localized 4f electron states and are coupled together via indirect exchange interactions involving the itinerant conduction electrons. Furthermore, even in a metal, the crystal-field energy levels for a rare-earth atom can readily be determined from inelastic neutron scattering experiments and, consequently, the magnetic polarization of the atom can be calculated as a function of the total effective (net exchange plus external) field, the temperature, and its orientation in the crystal. Such a procedure was followed in a recent study of a polycrystalline sample of PrAg, and the paramagnetic data revealed that the net exchange coupling in this intermetallic compound contains a higher-order (biquadratic) component comparable in strength to the normal bilinear component.²³

Our magnetic and neutron diffraction experiments have shown that the anomalous magnetic properties of PrAg below as well as above its Néel point can be directly attributed to the existence of biquadratic interactions.²⁴ Our magnetic studies have also revealed that strong biquadratic coupling exists in the compound, DySb.^{25,26}

EXPERIMENTAL RESULTS AND DISCUSSION

Transition-Group Alloys

During the contract period, our work pertinent to transition-group alloys consisted of the following: a detailed magnetization study of the Ni-Rh system near the critical composition for ferromagnetism and a similar but preliminary study of the Ni-Pd system; a study of the magnetic properties of Fe-Cr alloys near their critical temperatures; magnetization measurements on a Cu-Mn alloy near and below the freezing temperature for its micro-magnetic state.

Our magnetization studies of Ni-Rh began about five years ago, and the preliminary results of this work have already been reported.^{8,9} This investigation has subsequently been pursued in greater detail over a much broader range of alloy compositions, extending through the critical composition for ferromagnetism. The data analysis for this detailed investigation was completed about a year ago, and a full report of this work was recently published in the Physical Review;¹⁰ a reprint copy of this paper is attached as Appendix A.

In summary, our Ni-Rh results show that the paramagnetic susceptibility can be resolved into a Curie-Weiss component and a weakly temperature dependent component of the exchange-enhanced Pauli type. The onset of ferromagnetism is found to be directly related to a divergence of the Curie-Weiss susceptibility component and is attributed to interactions between superparamagnetic clusters. The average magnetic moment per cluster is deduced to

be $\sim 20-24 \mu_B$ over the composition range investigated (51-65 at.%Ni). The concentration of the magnetic clusters, though always dilute, increases rapidly as the critical composition is approached from the paramagnetic side. Moreover, the cluster concentrations correlate closely with the statistical occurrences of extremely Ni-rich local regions in these atomically disordered alloys. The intrinsically inhomogeneous paramagnetic and ferromagnetic states of Ni-Rh, thus described, are basically similar to those deduced earlier for Ni-Cu⁴ and Ni-V^{6,7} alloys near their critical compositions. These results disagree with previous speculation that the exchange enhancement in Ni-Rh does not become critical until ferromagnetic ordering takes place.²⁷ However, our evidence for the existence of giant-moment clusters in paramagnetic Ni-Rh, which presumably arise from critical local enhancement, is consistent with recent heat capacity measurements in a magnetic field.²⁸

Paramagnetic Ni-Pd alloys have been thought to provide an ideal isoelectronic situation for the occurrence of paramagnons (spin fluctuations) associated with a strong exchange enhancement at the Ni sites.²⁹ Indeed, the results of our preliminary magnetization study concur with this expectation for Ni-Pd alloys very dilute in Ni. However, as the critical composition for ferromagnetism is approached more closely, our results reveal the appearance of superparamagnetic clusters, which signifies that the local exchange enhancement at certain Ni atoms attains criticality even though the alloy remains magnetically disordered. Our

preliminary results on Ni-Pd were reported at the 1976 March Meeting of the American Physical Society; the abstract is attached as Appendix B.

We have measured the detailed magnetization-field-temperature properties of several Cr-rich Fe-Cr alloys close to their ferromagnetic Curie points. Our results show that the critical exponents have anomalous values, similar to those reported earlier for weakly ferromagnetic Pd-Fe³⁰ and Ni-Rh⁹ alloys. A further and more revealing similarity between the latter alloys and Fe-Cr was found in the values of the critical coefficients, which show that weakly ferromagnetic Fe-Cr alloys also have their magnetization distributed inhomogeneously in giant magnetic clusters. The results of this work were presented at the 1976 International Conference on Magnetism; a copy of the paper that appeared in the conference proceedings³¹ is attached as Appendix C.

In an investigation of Cu-Mn, we have explored the detailed magnetization-vs-field behavior of a ~20 at.%Mn alloy cooled in zero field to various temperatures. The temperature range of measurement extended through T_m , the so-called freezing temperature for the magnetomagnetic state, at which the initial susceptibility has a sharp maximum. Our results show T_m is also marked by a qualitative change in the nature of the magnetization processes. Below T_m , the changes in magnetization above a certain threshold field become irreversible, exhibiting hysteresis and remanence. The value of this threshold field and the amount of irreversibility

(i.e., the area of the hysteresis loops) both decrease gradually with increasing temperature and go to zero at T_m , above which the magnetization is reversible at all fields. In fact, it appears that the susceptibility peak at T_m is itself a manifestation of the onset of magnetic irreversibility, which is also suggested by recent work on Au-Fe.¹⁶ This effect is quite central and must be taken into account in any theoretical model for a spin-glass or mictomagnetic alloy.³² A brief report of our work was recently published in Solid State Communications;¹⁷ a copy of this paper is attached as Appendix D.

Rare-Earth Compounds

During the contract period, we have shown from theoretical analysis that the anomalous magnetic properties of the cubic (CsCl-type) compound PrAg can be explained on the basis of a strong biquadratic exchange coupling. Furthermore, we have completed a detailed magnetization study of the NaCl-structured compound DySb, whose magnetic properties suggest a similar predominance of higher-order (presumably biquadratic) exchange.

Our active interest in PrAg began shortly after neutron diffraction experiments³³ had shown this compound to be an antiferromagnet, contrary to previous reports of ferromagnetism, and had resulted in a determination of its crystal-field energy levels. We embarked on a magnetization study of a poly-crystalline sample of PrAg (since single crystals were then unavailable)

and our results, some of which have been briefly reported,²³ can be summarized as follows: PrAg is indeed an anti-ferromagnet with a Neel point (T_N) of $\sim 11^\circ\text{K}$. At all temperatures below T_N , it undergoes a spin-flop transition at a critical field (H_C) of $\sim 5 \text{ kOe}$. Above H_C , its magnetization (M) rises approximately as the cube root of the field (H), in contrast with the normal linear behavior. Moreover, the initial susceptibility increases anomalously below its peak at T_N . For the paramagnetic state above T_N , our M vs. H data were compared against M vs. H_{eff} (total effective field) calculated for the crystal-field states deduced from the neutron measurements.³³ Within the effective field approximation, $H_{\text{eff}} - H$ at a given M represents H_{exch} , the net exchange field on each Pr atom, and would normally be expected to vary linearly with M . Instead, we found that

$$H_{\text{exch}} \approx \lambda M + \lambda' M^3, \quad (1)$$

with λ' negative and of the same order of magnitude as λ .

In our analysis of this behavior, it was recognized that the $\lambda' M^3$ term in Eq. (1) can arise from a term in the exchange Hamiltonian that is quartic in the spin variables. The simplest such term has the isotropic biquadratic form $(\vec{S}_i \cdot \vec{S}_j)^2$. It was therefore assumed that the exchange Hamiltonian of the i th Pr atom interacting with j Pr neighbors may be written as

$$H_i = - \sum_j J_{ij} \vec{S}_i \cdot \vec{S}_j - \sum_j J'_{ij} (\vec{S}_i \cdot \vec{S}_j)^2 \quad (2)$$

where the first term on the right represents the usual bilinear exchange. Applying this Hamiltonian with negative J'_{ij} to the triplet ground state of PrAg (the excited states being ignorable except at very high temperatures) within the molecular field approximation, we found that Eq. (1) is totally justified for the paramagnetic state. Furthermore, this model Hamiltonian was found to generate all the anomalous antiferromagnetic properties of PrAg that are described above. A full report on this work, prepared in collaboration with T. O. Brun and G. H. Lander of the Argonne National Laboratory, was recently published in the Physical Review;²⁴ a copy of this paper is attached as Appendix E.

The compound DySb, which becomes antiferromagnetic at $T_N \approx 9^\circ\text{K}$ via a first-order transition, ^{34,35} undergoes rapid field-induced transitions whose characteristics depend on the crystallographic direction of the applied field.³⁶ With increasing field along $\langle 100 \rangle$, there is first a transition to a state whose magnetization corresponds to $\sim 5\mu_B/\text{Dy-atom}$ and then another to a state of $\sim 10\mu_B/\text{Dy-atom}$, corresponding to complete ferromagnetic alignment. The magnetization of the intermediate state suggests that half of the Dy^{3+} moments are parallel to the field and the other half are orthogonal.³⁶

From magnetization and neutron diffraction studies of a DySb crystal (the latter study conducted at the Argonne National Laboratory in collaboration with T. O. Brun and G. H. Lander),

we have determined the various magnetic states of this material and its magnetic phase diagrams for fields along different crystallographic directions. In particular, we have found that in the intermediate-field ordered state of DySb the magnetic moments do indeed form an orthogonal configuration, which can be attributed to strong biquadratic coupling of appropriate sign, i.e., J'_{ij} in Eq. (2) is negative, as in PrAg. The results of this work were presented at the 1974 Conference on Magnetism and Magnetic Materials and were published in the conference proceedings;²⁵ a copy of this paper is attached as Appendix F.

To further probe the existence of higher-order interactions in DySb, we pursued our detailed magnetization measurements throughout the paramagnetic regions of field and temperature. The paramagnetic data obtained, when analyzed as described above for PrAg, showed that the coefficient of the effective biquadratic coupling in DySb depends very sensitively on the temperature and on the crystallographic direction of the field. These results, which we are presently studying theoretically, were reported at the 1976 International Conference on Magnetism. A copy of the paper that appeared in the conference proceedings²⁶ is attached as Appendix G.

REFERENCES

1. T. J. Hicks, B. Rainford, J. S. Kouvel, G. G. Low, and J. B. Comly, Phys. Rev. Letters 22, 531 (1969).
2. C. G. Robbins, H. Claus, and P. A. Beck, Phys. Rev. Letters 22, 1307 (1969).
3. J. P. Perrier, B. Tissier, and R. Tournier, Phys. Rev. Letters 24, 313 (1970).
4. J. S. Kouvel and J. B. Comly, Phys. Rev. Letters 24, 598 (1970).
5. A. T. Aldred, B. D. Rainford, T. J. Hicks, and J. S. Kouvel, Phys. Rev. B 7, 218 (1973).
6. A. Amamou and B. Loegel, J. Phys. F 3, L79 (1973).
7. A. Amamou, F. Gautier, and B. Loegel, J. Phys. (Paris) 35, C4-217 (1974).
8. W. C. Muellner and J. S. Kouvel, Magnetism and Magnetic Materials--1971 (AIP Conf. Proc. No. 5, New York, 1972) p. 487.
9. W. C. Muellner and J. S. Kouvel, Solid State Commun. 15, 441 (1974).
10. W. C. Muellner and J. S. Kouvel, Phys. Rev. B 11, 4552 (1975).
11. J. W. Garland and A. Gonis, Magnetism in Alloys, edited by P. A. Beck and J. T. Waber (AIME, New York, 1972) p. 79.
12. K. Levin and D. L. Mills, Phys. Rev. B 9, 2354 (1974).
13. F. Gautier, F. Brouers, and J. Van Der Rest, J. Phys. (Paris) 35, C4-207 (1974).
14. H. Dvey-Aharon and M. Fibich, Phys. Rev. B 10, 287 (1974).
15. Spin glasses and mictomagnets were recently reviewed by J. A. Mydosh in Magnetism and Magnetic Materials-1974 (AIP Conf. Proc. No. 24, New York, 1975) p. 131.
16. J. L. Tholence and R. Tournier, J. Phys. (Paris) 35, C4-229 (1974).
17. H. Claus and J. S. Kouvel, Solid State Commun. 17, 1553 (1975).

18. J. S. Kouvel, J. Phys. Chem. Solids 21, 57 (1961); ibid, 24, 795 (1963).
19. P. A. Beck, Magnetism in Alloys, edited by P. A. Beck and J. T. Waber (AIME, New York, 1972) p. 211.
20. V. Cannella and J. A. Mydosh, Magnetism and Magnetic Materials - 1973 (AIP Conf. Proc. No. 18, New York, 1974) p. 651.
21. B. Window, Magnetism and Magnetic Materials 1, 167 (1975).
22. D. A. Smith, J. Phys. F 5, 2148 (1975).
23. T. O. Brun, J. S. Kouvel, G. H. Lander, and R. Aitken, Solid State Commun. 15, 1157 (1974).
24. T. O. Brun, J. S. Kouvel, G. H. Lander, Phys. Rev. B 13, 5007(1976).
25. T. O. Brun, G. H. Lander, F. W. Korty, and J. S. Kouvel, Magnetism and Magnetic Materials - 1974 (AIP Conf. Proc. No. 24, New York, 1975) p. 244.
26. J. S. Kouvel, T. O. Brun, and F. W. Korty, Physica 86-88B, 1043 (1977).
27. W. F. Brinkman, E. Bucher, H. J. Williams, and J. P. Maita, J. Appl. Phys. 39, 547 (1968).
28. B. B. Triplett and N. E. Phillips, Phys. Letters 37A, 443 (1971).
29. P. Lederer and D. L. Mills, Phys. Rev. 165, 837 (1968); Phys. Rev. Letters 20, 1036 (1968).
30. J. S. Kouvel and J. B. Comly, in Critical Phenomena in Alloys, Magnets, and Superconductors, R. E. Mills, E. Ascher, and R. I. Jaffee, eds. (McGraw-Hill, New York, 1971).
31. A. T. Aldred and J. S. Kouvel, Physica 86-88B, 329 (1977).
32. For various models proposed for the spin-glass or micro-magnetic state, see: J. S. Kouvel (Ref. 18); B. Window (Ref. 21); D. A. Smith (Ref. 22); K. Atkins and N. Rivier, J. Phys. (Paris) 35, C4-237 (1974); S. F. Edwards and P. W. Anderson, J. Phys. F 5, 965 (1975); D. Sherrington and S. Kirkpatrick, Phys. Rev. Letters 35, 1792 (1975).

33. T. O. Brun, G. H. Lander, D. L. Price, G. P. Felcher, and J. F. Reddy, Phys. Rev. B 9, 248 (1974).
34. E. Bucher, R. J. Birgeneau, J. P. Maita, G. P. Felcher, and T. O. Brun, Phys. Rev. Letters 28, 746 (1972).
35. G. P. Felcher, T. O. Brun, R. J. Gambino, and M. Kuznietz, Phys. Rev. B 8, 260 (1973).
36. G. Busch and O. Vogt, J. Appl. Phys. 39, 1334 (1968).

Magnetic properties of Ni-Rh alloys near the critical composition for ferromagnetism*

W. C. Mueller[†] and J. S. Kouvel

Department of Physics, University of Illinois, Chicago, Illinois 60680

(Received 22 January 1975)

The magnetizations of Ni-Rh alloys on either side of the critical composition for ferromagnetism ($c_{\text{crit}} \approx 63\text{-at.\% Ni}$) were measured between 4.2 and 250 °K in fields up to 56 kOe. The initial paramagnetic susceptibility of each alloy is shown to be resolvable into a Curie-Weiss component and a weakly temperature-dependent component of the exchange-enhanced Pauli type. The latter component, which is essentially equal to the high-field differential susceptibility at low temperatures, is maximum near c_{crit} . The onset of ferromagnetism, however, is more directly related to divergence of the Curie-Weiss susceptibility component and is attributed to interactions between superparamagnetic clusters. The average moment per cluster is deduced to be $\sim (20\text{--}24)\mu_B$ over the composition range investigated (65–51-at.\% Ni). The concentration of the magnetic clusters, though remaining dilute, increases rapidly as c_{crit} is approached from the paramagnetic side; moreover, it correlates closely with the statistical occurrence of extremely Ni-rich local regions in these atomically disordered alloys. Comparisons are made with the Ni-Cu and Ni-V systems near c_{crit} , for which recent magnetization studies have revealed the analogous existence of dilute concentrations of giant magnetic clusters.

INTRODUCTION

The alloys of nickel pose a special challenge to our understanding of magnetism in metallic systems. Historically, their spontaneous magnetizations and related properties were once thought to have found a simple explanation in the collective-electron rigid-band model, particularly in the case of nickel alloys with non-transition-group metals (Cu, Zn, etc.).¹ This theoretical rationale was applied fairly successfully to ferromagnetic alloys all the way out to the critical composition (c_{crit} , where the Curie point $T_C \rightarrow 0$ °K) and even beyond into the paramagnetic composition range, where the exchange forces are expected to cause an enhancement of the Pauli susceptibility. However, it has been known that certain detailed properties of the prototypal Ni-Cu system near c_{crit} (e.g., pronounced susceptibility increases at low temperatures,^{2,3} an essentially temperature-independent component of the specific heat^{4,5}) are distinctly anomalous from a rigid-band model viewpoint and are more readily attributable to superparamagnetic clusters acting as giant local moments.⁶ Generally, these anomalies have been dismissed as extraneous manifestations of gross chemical inhomogeneities in the alloy samples.⁷ The fact that Ni, as a dilute impurity in Cu or any other nonmagnetic metal host, shows no signs of having a stable local moment (unlike Fe or Mn)⁸ seemed to argue against the possibility of local moments as intrinsic phenomena in concentrated Ni alloys.

Many recent developments have changed this picture profoundly, especially with regard to Ni-Cu. Most recently, neutron scattering experiments on ferromagnetic Ni-Cu alloys by Aldred *et al.*⁹ (and

earlier on one alloy by Cable *et al.*¹⁰) have demonstrated that the 3d-electron moment of a Ni atom depends sensitively on its local environment, decreasing in magnitude with increasing number of neighboring Cu atoms. Indeed, these results⁹ indicate a gradual evolution with increasing Cu concentration toward the highly inhomogeneous spatial distributions of magnetization in the weakly ferromagnetic alloys near c_{crit} . These distributions, as deduced previously by Hicks *et al.* from similar experiments,¹¹ consist of discrete regions of magnetization, called "magnetic polarization clouds," each extending over many atoms and having an average total moment of about $10\mu_B$. Later susceptibility measurements on Ni-Cu revealed that the giant polarization clouds persist, as superparamagnetic entities, well into the paramagnetic composition range.¹² Moreover, the very dilute concentrations of these superparamagnetic clouds indicated that they nucleate at local regions that are extremely Ni rich. These local Ni-rich regions, the cores of the polarization clouds, may occur statistically even in perfectly random solid solutions, as has been discussed by Perrier *et al.*¹³; the short-range atomic clustering that normally exists in Ni-Cu alloys^{9,14} simply increases the concentration of these regions. This statistical picture, with the magnitude of each Ni atomic moment having a simple prescribed dependence on its local chemical environment, gives a good quantitative fit to the saturation magnetizations of Ni-Cu alloys near c_{crit} .¹³ An analogous but more complicated prescription adopted by Robbins *et al.*¹⁵ gives excellent agreement over the entire Ni-Cu composition range. This viewpoint of a spatially inhomogeneous magnetic state has been incorporated, often with some allowance for the magnetic aspects

of the local environments, into several theoretical analyses of the magnetization and related properties of Ni-Cu.¹⁶⁻²³

It has now begun to appear that the magnetism of other Ni-based alloy systems, not only of Ni-Cu, can be characterized near c_{crit} in terms of polarization clouds (often referred to as "magnetic clusters"). Among the evidence accumulating to this effect, probably the most convincing have again been the results of elastic neutron scattering experiments on weakly ferromagnetic alloys. These results have been reported for Ni-Pd,²⁴ Ni-Cr,²⁵ and Ni-Rh,²⁶ and in each case a marked upswing of the diffuse magnetic cross section at very small scattering vectors has signified the existence of moment-density distributions extending over many atomic volumes, each distribution constituting a magnetic cluster. The case of Ni-Rh is particularly interesting since Bucher *et al.*²⁷ have claimed, on the basis of a specific-heat and susceptibility study of this system, that the anomalies observed near c_{crit} (~63-at. % Ni) arise from a critical exchange enhancement accompanied by large spin fluctuations. Their low-temperature specific-heat results were later reanalyzed by Hahn and Wohlfarth²⁸ and shown to be equally consistent with the existence of superparamagnetic clusters, for which there also was some qualitative susceptibility evidence in alloys near c_{crit} .²⁹ More recently, Triplett and Phillips³⁰ found that the anomalous low-temperature component of the heat capacity of the alloy Ni₆₂Rh₃₈ is largely suppressed (probably shifted to higher temperatures) by the application of a 38-kOe field. They concluded that this observed effect is in good quantitative agreement with the predicted behavior of superparamagnetic clusters and, furthermore, that it would have required much larger fields if the anomalous heat capacity contribution were associated with spin fluctuations.

The existence of magnetic clusters in Ni-Rh clearly calls for more complete documentation in order to establish whether or not it is a significant intrinsic phenomenon. In view of this experimental need and the continued interest in Ni-Rh, we have carried out a systematic magnetization study of this alloy system near the critical composition for ferromagnetism (c_{crit}). Our preliminary results for a few paramagnetic Ni-Rh alloys, recently reported in brief,³¹ appear to indicate that magnetic clusters do indeed play an intrinsic role, qualitatively akin to their role in Ni-Cu. In the present paper, our complete results for a much broader range of Ni-Rh compositions, extending through c_{crit} , are described and discussed in full detail. Pertinent aspects of the magnetic critical-point behavior of the weakly ferromagnetic alloy Ni₅₅Rh₄₅, which we have reported separately,³² are also included in the present discussion.

EXPERIMENTAL TECHNIQUES

Nickel-rhodium alloy buttons were prepared by arc-melting weighed mixtures of the two metals (both specified as 99.999% pure) in a helium atmosphere and were cold worked by hammering. The samples machined from each button were cylinders (2.5 mm diam, 5 mm long) whose edges were beveled down in order to approximate ellipsoids (for reasonably uniform demagnetization). After their surfaces were acid etched, the samples were sealed in helium-filled quartz tubes, annealed for 3 days at 1200 °C, then quenched into water. The nominal compositions of the alloy samples are indicated in Table I. As later inferred from our susceptibility data, the ferromagnetic (presumably Fe) impurity level in the samples was probably well under 50 ppm.

Magnetization measurements on these samples were carried out with a temperature-controlled vibrating-sample magnetometer system (Princeton Applied Research Corp., Model No. 150-A). The Nb-Ti superconducting solenoid (Westinghouse Corp., Model No. H-5794) in this system was typically operated at currents up to 50 A corresponding to a maximum field at the sample of 56 kOe. The current-field specifications of the magnet were tested by means of a calibrated field-sensitive Bi-film resistor (American Aerospace Controls Corp., Model No. MRA-12); the field homogeneity over the sample length was found to be within 1%. The sample-zone temperature was monitored by a GaAs-diode thermometer (Lake Shore Cryotronics, Inc.), which we calibrated in zero field against a precalibrated Ge resistor (Cryocal, Inc., Model No. CR-1000) and a precalibrated Pt resistor (Minco Products, Inc., Model No. 51061-2) over the ranges (4.2–40)°K and (40–260)°K, respectively. Each temperature calibration point corresponded to a recorded setting of the temperature-control unit that governed the current to an electric heat exchanger (temperature monitored by another GaAs diode), through which vapor from the liquid-He reservoir flowed into the sample chamber at a controlled rate. Since the GaAs diodes were not entirely field insensitive, calibration corrections were determined as a function of field at various fixed temperatures set by means of a He-gas thermometer bulb inserted in the sample chamber. The maximum uncertainty in the sample temperature over the ranges of operation [(4.2–250)°K, 0–56 kOe] was about 0.1°K; the uncertainty was much less at 4.2°K, when the sample chamber was generally flooded with liquid He. The magnetic-moment calibration of the magnetometer output voltage was tested at different sensitivity levels against the saturation moments of various sized samples of pure Ni and Fe at 4.2°K.³³ The mag-

TABLE I. Magnetic properties of Ni-Rh alloys.

Alloy (at. % Ni)	$\sigma_0(0)$ (emu/g)	$\sigma_s(0)$ (emu/g)	T_C (°K)	σ (°K)	$\chi'(0)^a$	C_{CW}^b	$\bar{\mu}^*$ (μ_B)	\bar{c}^* (%)	P_{12} (%)
65.0	7.40	11.70	44	62	0.77	5.15	19.7	0.790	0.370
64.4	5.00	10.20	27	43	0.91	4.59	20.1	0.676	0.328
64.0	3.95	9.10	19	34	1.05	4.16	20.4	0.595	0.302
63.2	1.70	7.40	5	11	1.43	3.76	22.7	0.438	0.257
62.6	~0	5.80	~0	4	2.00	2.78	21.4	0.365	0.227
62.0	...	4.95	...	-2	2.22	2.29	20.7	0.324	0.200
60.0	...	3.40	...	-21	2.00	1.61	21.1	0.220	0.131
58.0	...	1.55	...	-43	1.76	0.826	23.8	0.090	0.084
56.0	...	0.96	...	-47	1.63	0.501	23.3	0.058	0.053
53.0	...	0.52	...	-43	1.33	0.263	22.6	0.033	0.026
51.0	...	0.33	...	-50	1.04	0.160	21.7	0.022	0.016
estimated uncertainties (\pm)									
0.1	2%	5%	0.5	2	5%	3%	8%	13%	...

^a $\chi'(0)$ and C_{CW} in units of 10^{-3} emu/Oe g and 10^{-3} emu °K/Oe g, respectively.

netization values for these samples checked within 1%, which represents the absolute error in all our magnetization measurements. The relative error in the magnetizations measured at different temperatures and fields for a given mounting of a sample was about an order of magnitude smaller.

EXPERIMENTAL RESULTS AND DISCUSSION

The magnetization (σ) of each Ni-Rh alloy sample was measured as a function of magnetic field (H , as corrected for demagnetization) at temperatures (T) from 4.2 °K up to about 250 °K. Our results for σ vs H at 4.2 °K are illustrated in Fig. 1. The curves for the alloys of 63.2-at. % or more Ni show a spontaneous magnetization (σ_0) clearly indicative of ferromagnetism. The Curie points (T_C) of these alloys were determined from isothermal σ^2 vs H/σ plots of the data; their values, together with those of σ_0 extrapolated to 0 °K, are listed in Table I. A similar plot for the 62.6-at. % Ni sample gives $T_C \approx 0$ °K, indicating that this alloy is essentially at the critical composition for ferromagnetism (c_{crit}). Moreover, the σ^2 vs H/σ plots near T_C , which are extremely sensitive to any macroscopic inhomogeneities, revealed no metallurgical complications in our alloy samples.

For each alloy over its paramagnetic range of temperatures, the initial susceptibility (χ_0) was determined from $d\sigma/dH$ extrapolated to $H=0$; its reciprocal values (χ_0^{-1}) are shown plotted versus T in Fig. 2. In their concave-downward shape (particularly evident at low temperatures), these curves agree with the earlier Ni-Rh results of Cottet *et al.*²⁹ They differ qualitatively from the flat concave-upward curves normally predicted from simple itinerant-electron band theory.¹ In this sense, the χ_0^{-1} vs T curves for Ni-Rh resemble those for paramagnetic Ni-Cu near c_{crit} , where the latter were

each found to be analyzable into a Curie-Weiss component and a weak temperature-independent component, attributed respectively to superparamagnetic clusters and itinerant-electron band polarization.¹²

Following an analogous procedure for Ni-Rh alloys near c_{crit} , we assume that the measured magnetization may be expressed as

$$\sigma(H, T) = \sigma_d(H, T) + H\chi'(T), \quad (1)$$

where σ_d represents the magnetization arising from the spin alignment of clusters and χ' is a band-polarization susceptibility, which is expected to be

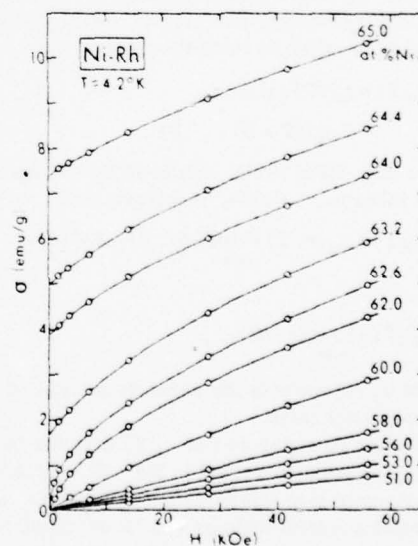


FIG. 1. Magnetization vs field at 4.2 °K for Ni-Rh alloys (compositions in at. % Ni).

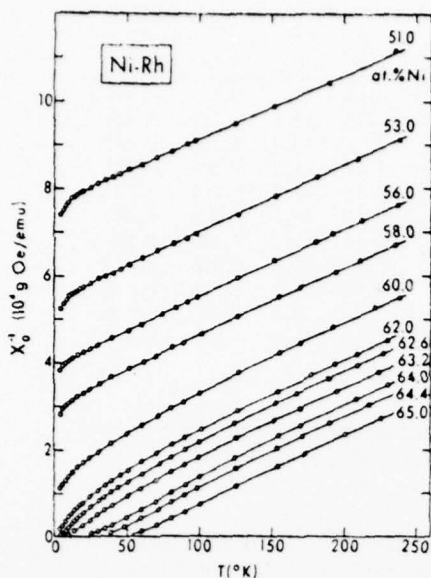


FIG. 2. Inverse initial susceptibility vs temperature for Ni-Rh alloys (compositions in at. % Ni).

only mildly temperature dependent and negligibly dependent on laboratory fields. Consequently, the spontaneous magnetization of a ferromagnetic alloy below T_c will derive entirely from the zero-field alignment of cluster moments, i. e., $\sigma_0(T) = \sigma_{cl}(0, T)$, whereas the initial susceptibility above T_c (and at all temperatures for a paramagnetic alloy) will include a band polarization term as well as a superparamagnetic cluster term, the latter of which is taken to be Curie-Weiss-like, i. e.,

$$\begin{aligned}\chi_0(T) &= \chi_{cl}(T) + \chi'(T) \\ &= C_{CW}/(T - \Theta) + \chi'(T).\end{aligned}\quad (2)$$

In the high-field limit, achieved by extrapolation from laboratory fields, it follows that

$$\sigma_s(T) \equiv \sigma_{cl}(\infty, T) = \lim_{H \rightarrow \infty} [\sigma(H, T) - H\chi'(T)] \quad (3)$$

and

$$\chi'(T) = \lim_{H \rightarrow \infty} (d\sigma/dH)_T, \quad (4)$$

where σ_s represents the saturation limit of the cluster spin alignment.

In order to separate our $\chi_0(T)$ data for Ni-Rh into the components indicated in Eq. (2), we took as an approximate low-temperature value for χ' the differential susceptibility at 4.2 °K extrapolated to infinite field, as suggested by Eq. (4). The value thus estimated was $\sim 2 \times 10^{-5}$ emu/Oeg for all the paramagnetic alloys. This starting value for χ' was then adjusted for each of these alloys until $(\chi_0 - \chi')^{-1}$

vs T became linear over a range of low temperatures (i. e., up to ~ 20 °K). In order that this linearity continue up to moderate temperatures (~ 100 °K), it was found necessary in each case to let χ' have a weak temperature dependence of the form

$$\chi'(T) = [\chi'^{-1}(0) + \alpha T^2]^{-1} \quad (5)$$

with α positive. At still higher temperatures, where the latter procedure began to overestimate the variation in χ' , we simply extended the linear dependence of $(\chi_0 - \chi')^{-1}$ on T and computed backwards to obtain the χ' values corresponding to the measured values of χ_0 . Our results for the temperature dependence of $\chi_{cl}^{-1} \equiv (\chi_0 - \chi')^{-1}$ and of χ'^{-1} are plotted in Figs. 3(a) and (b), respectively; the values of $\chi'(0)$ are listed in Table I. For the ferromagnetic alloys, since the above analysis cannot be used below T_c , we adjusted $\chi'(0)$ to the values listed in Table I and assumed that $\chi'^{-1}(T)$ is displaced upward uniformly from the curve determined for the critical-composition (62.6-at. % Ni) alloy, as illustrated in Fig. 3(b). The linear plots thus obtained for $\chi_{cl}^{-1}(T)$ above T_c , which are presented in Fig. 3(a), are rather insensitive to the exact shape assumed for $\chi'^{-1}(T)$ owing to the fact that χ' is only a small part of χ_0 over this temperature range.

For each Ni-Rh alloy, the values of C_{CW} and Θ obtained from the Curie-Weiss behavior of $\chi_{cl}(T)$, as expressed in Eq. (2), are listed in Table I. Allowing that χ_{cl} is associated with superparamagnetic clusters, we can write for the Curie-Weiss constant

$$C_{CW} = Nc^* \langle \mu^{*2} \rangle / 3k, \quad (6)$$

where N is the number of atoms per gram, c^* the cluster concentration (number per atom), $\langle \mu^{*2} \rangle$ the mean squared value of the magnetic moment per cluster, and k the Boltzmann constant. We further allow that the saturation magnetization $\sigma_s(0)$ obtained by high-field extrapolation of $\sigma(H, 0) - H\chi'(0)$, as indicated in Eq. (3), represents the parallel spin alignment of all the magnetic clusters in the alloy and can therefore be expressed as

$$\sigma_s(0) = Nc^* \langle \mu^* \rangle. \quad (7)$$

Typical high-field extrapolations for the Ni-Rh alloys, involving our low-temperature magnetization data (extended trivially to 0 °K) and the values deduced for $\chi'(0)$, are illustrated in Fig. 4. The values thus determined for $\sigma_s(0)$ are listed in Table I. From a combination of Eqs. (6) and (7), we obtain the "average" quantities defined as

$$\bar{\mu}^* \equiv \langle \mu^{*2} \rangle / \langle \mu^* \rangle = 3kC_{CW} / \sigma_s(0), \quad (8a)$$

$$\bar{c}^* \equiv c^* \langle \mu^* \rangle / \bar{\mu}^* = \sigma_s^2(0) / 3NkC_{CW}. \quad (8b)$$

(Note that a distribution in cluster moment size will

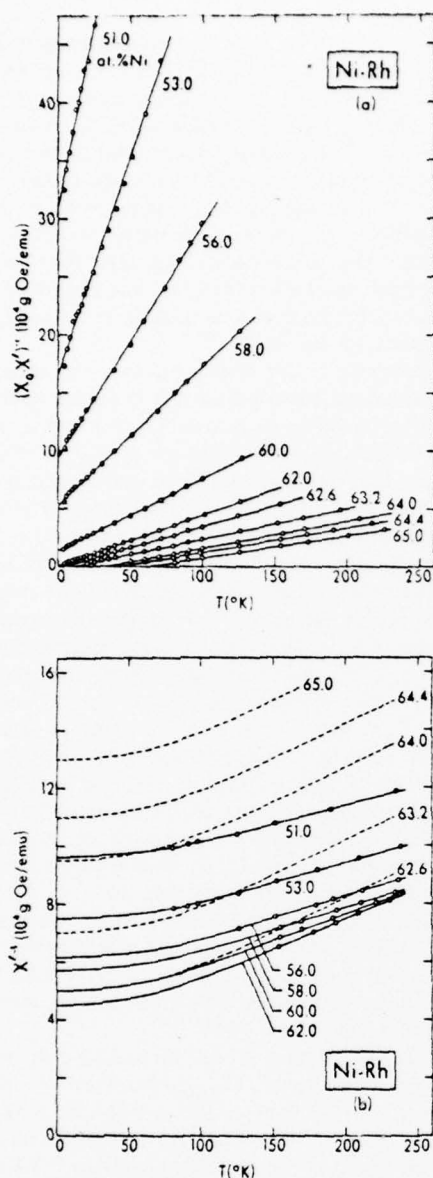


FIG. 3. (a) Inverse of $\chi_{el} \equiv \chi_0 - \chi'$ and (b) inverse of χ' , as functions of temperature, for Ni-Rh alloys (compositions in at. % Ni).

affect the meaning of $\bar{\mu}^*$ and \bar{c}^* , rendering them respectively higher and lower than the true average values, $\langle \mu^* \rangle$ and $\langle c^* \rangle$. Substituting our experimentally derived values for C_{CW} and $\sigma_s(0)$ into these expressions, we calculated the $\bar{\mu}^*$ and \bar{c}^* values listed in Table I. From these results we see that the cluster moment $\bar{\mu}^*$ has enormous values [$\sim (20-24)\mu_B$] that are remarkably constant over the composition range of study. Contrastingly, the cluster concentrations \bar{c}^* are very small and de-

crease rapidly with decreasing at. % Ni, passing smoothly through the critical composition. Qualitatively, these results for the average moment and concentration of magnetic clusters in Ni-Rh are very similar to those previously obtained for¹² Ni-Cu and³⁴ Ni-V by the same method of data analysis, which yielded giant $\bar{\mu}^*$ values of $\sim 10\mu_B$ and $\sim 40\mu_B$, respectively, near c_{crit} .

Evidence for giant magnetic clusters in the weakly ferromagnetic $\text{Ni}_{45}\text{Rh}_{55}$ alloy was also extracted from detailed $\sigma(H, T)$ data in the vicinity of T_C , as we have already reported separately.³² From these data, the spontaneous magnetization just below T_C and the initial susceptibility just above T_C were determined and their temperature dependences described respectively as $\sigma_0(T) = m_0 |1 - T/T_C|^\beta$ and $\chi_0(T) = (m_0/h_0) |1 - T/T_C|^{-\gamma}$, where β and γ are critical exponents, and m_0 and m_0/h_0 may be regarded as critical coefficients. Our results for the latter were compared with the theoretical predictions that $m_0/\sigma_0(0) = n_1$ and $\mu_0 h_0/kT_C = n_2$, in which the elementary moment μ_0 is normally taken to be the average moment per atom and the numbers n_1 and n_2 are both slightly larger than unity for various classic models (mean field, Ising). While our experimental value for n_1 obeyed these predictions quite well, the value for n_2 was only ~ 0.007 when μ_0 was equated to $\sigma_0(0)/N \approx 0.1\mu_B$. Indeed, agreement with the near-unity values predicted for n_2 required that we set $\mu_0 \approx 22\mu_B$, which is essentially the $\bar{\mu}^*$ value for this alloy given in Table I. Thus, it was concluded that the elementary dynamical moments involved in the Curie-point transition are those of giant magnetic clusters rather than of in-

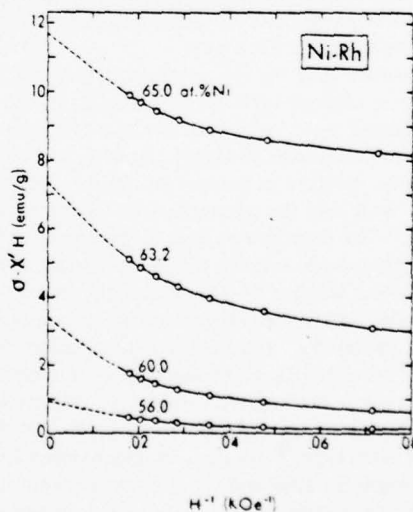


FIG. 4. Variation of $\sigma - \chi'H$ (for $T = 0^\circ\text{K}$) with H^{-1} for Ni-Rh alloys (compositions in at. % Ni).

dividual atoms. We further showed that the same conclusion can be reached analogously from the Curie-point properties of dilute PdFe, the classic giant-moment alloys—whose critical exponent values, incidentally, also are anomalous and similar to those of the Ni-Rh alloy.

As was done in the case of Ni-Cu,¹² let us examine the possibility that the magnetic cluster concentrations in Ni-Rh correlate with the statistical occurrences of a particular local chemical composition. For simplicity, consider the probability P_n that any lattice site of a fcc Ni_cRh_{1-c} alloy (assumed to be a random solid solution) is occupied by a Ni atom whose 12 nearest neighbors include n or more Ni atoms. In the extreme case of $n = 12$, we have $P_{12} = c^{12}$, whose values for the alloys studied are listed in Table I. The variation of P_{12} with alloy composition is clearly quite similar to that of \bar{c}^* , although at the Ni-rich end of this range the values of \bar{c}^* appear to be rising towards $P_{11} = c^{12} + 12c^{11}(1-c)$, whose values exceed those of P_{12} by nearly an order of magnitude. Despite the oversimplicity of these considerations, they are probably correct in indicating that the giant magnetic clusters in Ni-Rh are nucleated in local regions that are extremely Ni rich. In the case of Ni-Cu, \bar{c}^* was originally found¹² to lie between P_{10} and P_{11} , but it was recently shown²⁰ in a more rigorous statistical treatment of the atomic clustering that \bar{c}^* follows closely the values of P_{12} . Thus, the local conditions for magnetic cluster nucleation in Ni-Rh and Ni-Cu appear to be fairly alike. In either case, according to the neutron diffraction work on Ni-Rh,²⁶ and Ni-Cu,¹¹ the average moment density inside a magnetic cluster decreases gradually over a radial distance of many lattice spacings and thus extends considerably outside the central core of nearest-neighbor Ni atoms.

Whatever may be the underlying mechanisms for magnetic cluster formation in Ni-Rh (which will be commented upon later), it is clear from our results that giant magnetic clusters persist, as superparamagnetic entities in extremely dilute concentrations, well into the paramagnetic composition range. The negative values of the Curie-Weiss temperature (Θ) for the weakly paramagnetic Ni-Rh alloys, similar to (though larger in magnitude than) the negative Θ values for paramagnetic Ni-Cu,¹² and Ni-V,³⁴ may reflect local anisotropy effects³⁵ as much as a predominance of antiferromagnetic over ferromagnetic exchange interactions, presumably of the indirect Ruderman-Kittel-Kasuya-Yosida type.¹⁸ As c_{crit} is approached from the paramagnetic side and the cluster concentration in Ni-Rh increases, Θ rises sharply to large positive values, probably as the outcome of increased ferromagnetic (direct overlap) interactions between adjacent clusters. Beyond c_{crit} , in the weakly ferro-

magnetic Ni-Rh alloys, the spontaneous magnetization $\sigma_0(0)$ is much smaller than the corresponding saturation value $\sigma_s(0)$, although their ratio does approach unity with increasing at.% Ni, as seen in Table I. This behavior shows that in zero external field many of the magnetic clusters in these alloys are not ferromagnetically aligned even at very low temperatures—which is consistent with the fact that specific-heat anomalies of the type ascribable to superparamagnetic clusters²⁸ are observed in the weakly ferromagnetic as well as the strongly paramagnetic Ni-Rh alloys.²⁷

According to our interpretation, the onset of ferromagnetism in Ni-Rh arises from the exchange coupling between magnetic clusters and is manifested at T_C in the divergence of χ_{cl} , the Curie-Weiss-like cluster component of the initial susceptibility, as indicated in Fig. 3(a). The other component of the initial susceptibility (i.e., χ') exhibits only a mild T^2 deviation from its zero-temperature value and, as further seen from Fig. 3(b), the variation of χ'^{-1} at higher temperatures seems to approach a weak linear dependence. A very similar behavior was recently deduced for χ' vs T in Ni-V alloys close to the critical composition,³⁴ for which $\chi'(0)$ is comparable in size to our Ni-Rh results. Values obtained for χ' in Ni-Cu alloys near c_{crit} are about an order of magnitude smaller and were assumed to have negligible temperature dependence¹²; they were attributed, as was mentioned earlier, to weak band polarization effects. In the case of Ni-Rh, the χ'^{-1} vs T curves in Fig. 3(b) have exactly the shape predicted for such effects when the exchange enhancement is large and accompanied by spin fluctuations.³⁶ An analogous explanation was given for the similar χ'^{-1} vs T curves for Ni-V.³⁷

Our $\chi'(0)$ results for Ni-Rh are plotted versus alloy composition in Fig. 5, together with $d\sigma/dH$ values taken at various fields from the σ vs H curves for 4.2°K in Fig. 1. The peaks in the $d\sigma/dH$ curves at the critical composition (~63-at.% Ni), which are most prominent at the lowest fields, are clearly the vestiges of the divergence of $d\sigma/dH$ at zero field. Hence, they relate more closely to the magnetic cluster component of the initial susceptibility (i.e., χ_{cl}) than to the band polarization component (χ'), and this appears to be true even at the highest fields where, according to Eq. (4), $d\sigma/dH$ should be extrapolating to χ' . It is evident from Fig. 5 that the high-field approach of $d\sigma/dH$ to χ' is extremely slow in all these alloys, not only in those very close to c_{crit} . This behavior quite possibly derives from a broad distribution in the magnetic moments of the individual clusters, in which case the clusters with relatively small moments continue to contribute to the low-temperature differential susceptibility up to very high fields.

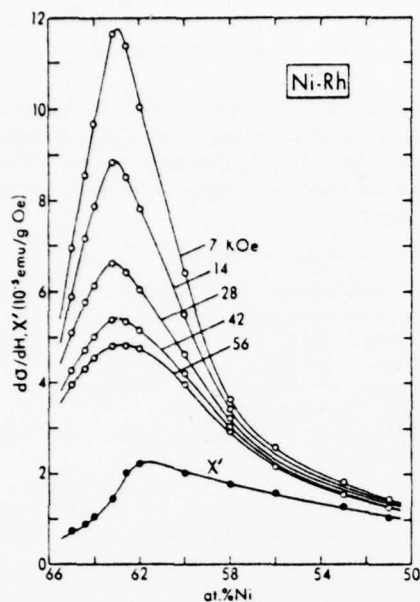


FIG. 5. Open circles: $d\sigma/dH$ at various fields (in kOe) at 4.2°K; closed circles: $\chi'(0)$, as functions of Ni-Rh alloy composition.

Cluster moment distributions in³⁸ Ni-Cu and³⁴ Ni-V have been proposed on the basis of similar experimental evidence.

The variation of our results for $\chi'(0)$ is shown in Fig. 6 with respect to the entire Ni-Rh composition range. On this scale, the values for $\chi'(0)$ define a sharp but finite peak centered near the critical composition. Their rapid decrease on the Rh-rich side of the peak extends smoothly through the points representing some previous high-field susceptibility data,²⁷ which at these compositions can be safely assumed to contain virtually no magnetic cluster contribution. The descent of $\chi'(0)$ on the Ni-rich side of the peak appears to be even faster, probably reaching very low values for most of the ferromagnetic range, as indicated in the figure. This behavior suggests that the band polarization effects that produce χ' , though not responsible for the onset of ferromagnetism, become highly exchange enhanced in the vicinity of c_{crit} . It seems reasonable to associate this strong exchange enhancement with local (presumably fairly Ni rich) regions that are nearly unstable towards the formation of local (cluster) moments. As implied by our χ' results in Fig. 6, these local regions grow and approach critical enhancement as the alloy composition increases in at.% Ni, but at c_{crit} they suddenly become exchange-polarized by the spontaneously aligned moments of the stable magnetic clusters

and, as a result, their contribution to the susceptibility (χ') drops precipitously. Spin fluctuations can be expected to occur in these regions of strong local enhancement and in fact, according to a recent resistivity study,³⁹ they appear to provide the dominant scattering mechanism in Ni-Rh alloys near c_{crit} . In the case of Ni-V, where χ' attains values comparable to those in Ni-Rh, the observed temperature dependence of the resistivity was also found to be characteristic of spin-fluctuation scattering³⁴; as in Ni-Rh, any scattering from the superparamagnetic clusters seems to be completely obscured. However, in the case of Ni-Cu, where χ' is very much weaker, the measured resistivity versus temperature curves indicate that the predominant scattering is from superparamagnetic clusters,⁴⁰ as was recently elucidated theoretically.²¹

Having attributed the $\chi'(0)$ peak in Fig. 6 to regions of near-critical exchange enhancement, we would be consistent in regarding each statistical Ni-rich local region that constitutes the core of a magnetic cluster in Ni-Rh as having reached and exceeded critical enhancement. There would consequently exist stable local moments on all the Ni atoms (and perhaps the Rh atoms as well)⁴¹ within each cluster core. From this point of departure in the case of Ni-Cu, Roth has proceeded to show analytically that the Ni atoms outside the core of a magnetic cluster will become magnetically polarized but to a decreasing extent with increasing distance from the core.¹⁷ This picture of a giant magnetic cluster or polarization cloud in Ni-Cu agrees with the spin density distribution deduced from

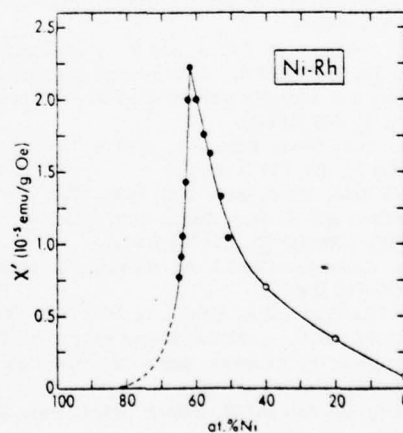


FIG. 6. Closed circles: $\chi'(0)$ vs Ni-Rh alloy composition; open circles: high-field susceptibility data from Ref. 27.

neutron diffraction data and has subsequently been described by Garland and Gonis in a self-consistent theoretical treatment of the entire magnetic cluster (core and all).²⁰ The cooperative magnetic processes invoked in the latter work are presumably also responsible for the giant magnetic clusters in Ni-Rh, but this remains to be investigated.

ACKNOWLEDGMENTS

The authors wish to thank Dr. H. Claus and Dr. J. W. Garland for many helpful discussions and suggestions. To Dr. Garland, we are also grateful for his critical reading of the manuscript of this paper.

- *This work was supported by the Research Board of the University of Illinois at Chicago Circle and, during its final stages, by the National Science Foundation and the Office of Naval Research.
- †Present address: Morton College, Cicero, Ill. 60650.
- ¹E. C. Stoner, *J. Phys. Radium* **12**, 372 (1951), and references therein.
 - ²F. M. Ryan, E. W. Pugh, and R. Smoluchowski, *Phys. Rev.* **116**, 1106 (1959).
 - ³H. C. Van Elst, B. Lubach, and G. J. Van den Berg, *Physica (Utr.)* **28**, 1297 (1962).
 - ⁴G. L. Guthrie, S. A. Friedberg, and J. E. Goldman, *Phys. Rev.* **113**, 45 (1959).
 - ⁵K. P. Gupta, C. H. Cheng, and P. A. Beck, *Phys. Rev.* **133**, A203 (1964).
 - ⁶K. Schröder, *J. Appl. Phys.* **32**, 880 (1961).
 - ⁷For a recent review of superparamagnetism in alloys, see J. S. Kouvel, *Magnetism in Alloys*, edited by P. A. Beck and J. T. Waber (AIME, New York, 1972), p. 165.
 - ⁸D. K. Wohlleben and B. R. Coles, *Magnetism*, edited by G. T. Rado and H. Suhl (Academic, New York, 1973), Vol. V, p. 3.
 - ⁹A. T. Aldred, B. D. Rainford, T. J. Hicks, and J. S. Kouvel, *Phys. Rev. B* **7**, 218 (1973).
 - ¹⁰J. W. Cable, E. O. Wollan, and H. R. Child, *Phys. Rev. Lett.* **22**, 1256 (1969).
 - ¹¹T. J. Hicks, B. Rainford, J. S. Kouvel, G. G. Low, and J. B. Comly, *Phys. Rev. Lett.* **22**, 531 (1969).
 - ¹²J. S. Kouvel and J. B. Comly, *Phys. Rev. Lett.* **24**, 598 (1970).
 - ¹³J. P. Perrier, B. Tissier, and R. Tournier, *Phys. Rev. Lett.* **24**, 313 (1970).
 - ¹⁴B. Mozer, D. T. Keating, and S. C. Moss, *Phys. Rev.* **175**, 868 (1968).
 - ¹⁵C. G. Robbins, H. Claus, and P. A. Beck, *Phys. Rev. Lett.* **22**, 1307 (1969). An improved version of this scheme was recently presented by S. Mishra [*Int. J. Magn.* **5**, 363 (1974)].
 - ¹⁶D. J. Kim, *Phys. Rev. B* **1**, 3725 (1970); *J. Phys. (Paris)* **32**, C1-755 (1971).
 - ¹⁷L. M. Roth, *Phys. Rev. B* **2**, 740 (1970).
 - ¹⁸M. Fibich and A. Ron, *Phys. Rev. Lett.* **25**, 296 (1970); *J. Phys. (Paris)* **32**, C1-748 (1971).
 - ¹⁹K. H. Bennemann and J. W. Garland, *J. Phys. (Paris)* **32**, C1-750 (1971).
 - ²⁰J. W. Garland and A. Gonis, in Ref. 7, p. 79.
 - ²¹K. Levin and D. L. Mills, *Phys. Rev. B* **9**, 2354 (1974).
 - ²²F. Gautier, F. Brouers, and J. Van Der Rest, *J. Phys. (Paris)* **35**, C4-207 (1974).
 - ²³H. Dvey-Aharon and M. Fibich, *Phys. Rev. B* **10**, 287 (1974).
 - ²⁴A. T. Aldred, B. D. Rainford, and M. W. Stringfellow, *Phys. Rev. Lett.* **24**, 897 (1970).
 - ²⁵B. D. Rainford, A. T. Aldred, and G. G. Low, *J. Phys. (Paris)* **32**, C1-575 (1971).
 - ²⁶A. T. Aldred and B. D. Rainford (private communication). Preliminary neutron-diffraction results on Ni-Rh were described qualitatively in Ref. 11.
 - ²⁷E. Bucher, W. F. Brinkman, J. P. Maita, and H. J. Williams, *Phys. Rev. Lett.* **18**, 1125 (1967); W. F. Brinkman, E. Bucher, H. J. Williams, and J. P. Maita, *J. Appl. Phys.* **39**, 547 (1968).
 - ²⁸A. Hahn and E. P. Wohlfarth, *Helv. Phys. Acta* **41**, 857 (1968).
 - ²⁹H. Cottet, P. Donzé, J. Ortelli, E. Walker, and M. Peter, *Helv. Phys. Acta* **41**, 755 (1968).
 - ³⁰B. Triplett and N. E. Phillips, *Phys. Lett. A* **37**, 443 (1971).
 - ³¹W. C. Mueller and J. S. Kouvel, *AIP Conf. Proc.* **5**, 487 (1972).
 - ³²W. C. Mueller and J. S. Kouvel, *Solid State Commun.* **15**, 441 (1974).
 - ³³The saturation-magnetization values adopted, 58.57 emu/g for Ni and 221.71 emu/g for Fe, were taken from H. Danan, A. Herr, and A. J. P. Meyer, *J. Appl. Phys.* **39**, 669 (1968).
 - ³⁴A. Amamou and B. Loegel, *J. Phys. F* **3**, L79 (1973); A. Amamou, F. Gautier, and B. Loegel, *J. Phys. (Paris)* **35**, C4-217 (1974).
 - ³⁵A recent unpublished analysis by H. Claus and one of us (J. S. K.) has revealed that a randomly oriented local anisotropy in a system of noninteracting superparamagnetic clusters can give rise to an apparent Curie-Weiss-like susceptibility with a negative value of Θ , when expressed as in Eq. (2), as well as to a low-temperature specific-heat anomaly of the type reported for Ni-Rh in Refs. 27 and 30.
 - ³⁶A. B. Kaiser and S. Doniach, *Int. J. Magn.* **1**, 11 (1970).
 - ³⁷In the second paper of Ref. 34, the χ' component of the susceptibility of Ni-V was subdivided into a temperature-independent part and a part whose variation with temperature is of the type reported here for χ' in Ni-Rh; the two parts were attributed respectively to "non-magnetic" and "nearly magnetic" atoms.
 - ³⁸S. Mishra and P. A. Beck, *Int. J. Magn.* **4**, 277 (1973).
 - ³⁹R. W. Houghton, M. P. Sarachik, and J. S. Kouvel, *Solid State Commun.* **10**, 369 (1972).
 - ⁴⁰R. W. Houghton, M. P. Sarachik, and J. S. Kouvel, *Solid State Commun.* **8**, 943 (1970); *Phys. Rev. Lett.* **25**, 238 (1970).
 - ⁴¹The fact that dilute NiRh alloys have a larger average ferromagnetic moment per atom than pure Ni metal [J. Crangle and D. Parsons, *Proc. R. Soc. A* **255**, 509 (1960)] would suggest that Rh atoms in a Ni-rich local environment may carry a substantial moment. Alternatively (or in addition), these Rh atoms may cause an increase of the moments of their neighboring Ni atoms, which would be analogous to the situation in dilute NiPd alloys deduced from neutron-diffraction data [J. W. Cable and H. R. Child, *Phys. Rev. B* **1**, 3809 (1970)].

Abstract Submitted
for the 1976 March Meeting of the
American Physical Society
29 March - 1 April 1976

Physics and Astronomy
Classification Scheme
Number: 75.30

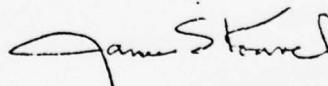
Bulletin Subject Heading
for Placement of Paper:
Magnetism

Giant Moments in Paramagnetic Pd-Ni Alloys*

D. SAIN and J. S. KOUVEL, Univ. of Illinois, Chicago --
For Pd-Ni alloys approaching the critical composition for
ferromagnetism (~ 2.5 at.% Ni) the initial susceptibility
as a detailed function of temperature T can be resolved
into a Curie-Weiss component, $\chi_{cw} = C_{cw}/(T-\theta)$, and a com-
ponent χ' whose weak dependence on T is characteristic of
unstable (fluctuating) moments. Up to ~ 1.8 at.% Ni,
where $\chi'(0^\circ\text{K})$ reaches a maximum, C_{cw} increases slowly and
is consistent with giant moments associated with the iron
impurity atoms (~ 80 ppm) in the alloys. Above 1.8 at.%
Ni, both C_{cw} and the saturation magnetization at 4.2°K
rise very rapidly and are attributable to an increasing
concentration of giant-moment clusters centered at small
statistical groups of neighboring Ni atoms. The values
of θ are extremely small ($< 0.1^\circ\text{K}$) up to 2.1 at.% Ni and
become increasingly positive as the critical composition
is approached more closely.

*Work supported by the National Science Foundation and
the Office of Naval Research.

Submitted by



James S. Kouvel

Department of Physics
University of Illinois
Chicago, Illinois 60680

Appendix C

CRITICAL MAGNETIC PROPERTIES OF Fe-Cr ALLOYS*

A.T. ALDRED

Argonne National Laboratory, Argonne, Illinois 60439, USA

and

J.S. KOUVEL†

University of Illinois, Chicago, Illinois 60680, USA

Detailed magnetization-field-temperature measurements on Cr-rich Fe-Cr alloys near their ferromagnetic Curie points reveal anomalous values for the critical exponents. From the values for the critical coefficients, it is deduced that the alloys are giant-moment systems, similar to Pd-Fe and Ni-Rh.

1. Introduction

The bulk magnetic properties [1,2] of Fe-Cr alloys containing greater than 30 at.% Fe indicate that the alloys are normal ferromagnets, and extrapolation of the data to higher chromium concentrations suggests that long-range ferromagnetic order should disappear in the region 15–20 at.% Fe. Neutron-diffraction experiments [3] imply that in this critical concentration region the magnetic moments will be confined primarily to the iron atoms, with a magnitude that will vary profoundly as a function of the local atomic environment. By analogy with the Ni-Cu system [4], we would thus anticipate the presence of giant moments in the critical concentration range centered about iron-rich clusters.

Earlier studies [5–8] of the magnetic properties of Fe-Cr alloys near the critical concentration do indicate that the distribution of magnetization is inhomogeneous. However, it is not clear whether the various results are self-consistent and whether the alloys can be described as ferromagnetic or mictomagnetic. The presence of short-range chemical inhomogeneities in the Fe-Cr system [3] complicates this problem, inasmuch as no two nominally-identical alloys prepared on separate occasions will ever have precisely the same atomic distribution and, therefore, the same magnetic properties.

In the present investigation, we have determined the detailed magnetic properties of Fe-Cr alloys containing 30, 25, and 20 at.% Fe in the

vicinity of the Curie temperature T_c . The primary aim, following the study of Kouvel and Comly [9], has been to determine the magnetic entity taking part in the ordering process and relate this to the anticipated 'giant moment'.

2. Experimental procedure and results

The alloys were prepared by arc melting the requisite amounts of 99.99 wt.% pure iron and chromium in a helium-argon atmosphere. After suitable heat treatment [2], samples were ground in the form of prolate ellipsoids ($\sim 5 \text{ mm} \times \sim 2 \text{ mm}$) and reannealed at 900°C for one day. Chemical analysis, and X-ray lattice parameter and density determinations all indicated that, within error, the actual and nominal compositions were the same.

A series of magnetic isotherms [specific magnetization σ (emu/g) as a function of internal field H (Oe)] was determined at 1 K intervals by the Faraday method in an apparatus already described [10]. As a function of both increasing and decreasing applied field in the range 0.25–14 kOe, the data yielded a set of smooth curves when plotted as σ^2 versus H/σ .

Extrapolation of these curves to the axes gave the inverse initial susceptibility $\chi_0^{-1}(T > T_c)$ and the square of the spontaneous magnetization $\sigma_s^2(T < T_c)$. Analysis of the temperature dependence of these quantities determined T_c and the critical exponents γ and β defined by:

$$\sigma_s^2 = m_0^2 \epsilon^{2\beta} \quad \text{and} \quad \chi_0^{-1} = (h_0/m_0) \epsilon^\gamma, \quad (1,2)$$

where $\epsilon = |1 - T/T_c|$, and m_0^2 and h_0/m_0 are critical coefficients. The critical isotherm

* Work supported by the US Energy Research and Development Administration.

†Supported in part by NSF and ONR.

Table I
Magnetic critical-point parameters for the alloys listed

	Fe ₁₀ Cr ₉₀	Fe ₂₅ Cr ₇₅	Fe ₃₀ Cr ₇₀	Ni ₈₅ Rh ₁₅	Pd _{98.6} Fe _{1.4}	Ni
T_c (K)	250(1)*	154(1)	64(2)	44.2	50.2	627.4
σ_0 (emu/g)	57.6	42	18	7.40	6.85	58.57
$\bar{\mu}_0$ (μ_B /at.)	0.548	0.40	0.17	0.098	0.130	0.616
β	0.44(1)	0.47(3)	0.52(1)	0.476	0.464	0.378
γ	1.82(1)	2.03(4)	2.12(1)	1.50	1.40	1.34
δ	5.15(3)	5.32(3)	5.11(3)	4.15	4.06	4.58
δ_{calc}	5.18	5.30	5.10	4.15	4.02	4.54
m_0 (emu/g)	63.6	47.2	26.8	8.66	8.25	83.3
h_0 (kOe)	509	236	28	48.3	132	15720
m_0/σ_0	1.10	1.12	1.3	1.17	1.20	1.42
$\bar{\mu}_0 h_0/kT_c$	0.075	0.044	0.0041	0.0072	0.023	1.04
μ^* (μ_B)	12	16	55	22	9	-
c^* (%)	4.6	2.6	0.31	0.45	1.4	-

* Numbers in parentheses represent estimated uncertainties in least significant figure.

($T = T_c$) was then plotted as $\log \sigma$ versus $\log H$ to give the exponent δ ($\sigma \propto H^{1/\delta}$).

The values obtained for the various parameters are listed in table I, together with comparative results for Ni [11], a Pd_{98.6}Fe_{1.4} alloy [9], and a Ni₈₅Rh₁₅ alloy [12]. The unusual exponent values found in this study, particularly for γ , may be related, by analogy with previous results [9, 12], to an inhomogeneous distribution of magnetization. In all cases, the exponents conform to the scaling relation $\delta = 1 + \gamma/\beta$, as

shown by the value of δ calculated in this manner from the γ and β values given in table I. The present data also obey the homogeneous equation of state, as shown by fig. 1 where some of the results for the Fe₂₅Cr₇₅ sample are plotted [9, 12] as m^2 ($\equiv \sigma^2 \epsilon^{-2\beta}$) versus h/m ($\equiv (H/\sigma) \epsilon^\gamma$).

3. Discussion

The intercepts of the curves in fig. 1 with the axes determine the coefficients m_0^2 and h_0/m_0 in eqs. (1) and (2), and these may be combined to yield m_0 and h_0 which are listed in table I. Also listed are the normalized quantities m_0/σ_0 and $\bar{\mu}_0 h_0/kT_c$, where σ_0 is the spontaneous magnetization at absolute zero and $\bar{\mu}_0$ is the corresponding mean moment per atom. The uncertainty in the σ_0 values for the 20 and 25 at.% Cr samples arises from the pronounced field dependence of the magnetization even at low temperatures which made a reliable extrapolation to $H = 0$ difficult. Although the values of m_0/σ_0 are close to previous results and theoretical estimates [9, 12], the values of $\bar{\mu}_0 h_0/kT_c$ are more than an order of magnitude less than theoretical values, as in the case of Pd_{98.6}Fe_{1.4} [9] and Ni₈₅Rh₁₅ [12]. Following previous work [9, 12], we define μ^* as the effective elementary moment taking part in the ordering process, and equate $\mu^* h_0/kT_c$ with the theoretical estimate (~ 1.6 [12]) to obtain values of μ^* the giant moment which are given in table I. Furthermore, if the concentration of these entities is c^* , then $\bar{\mu}_0 = \mu^* c^*$ and values of c^*

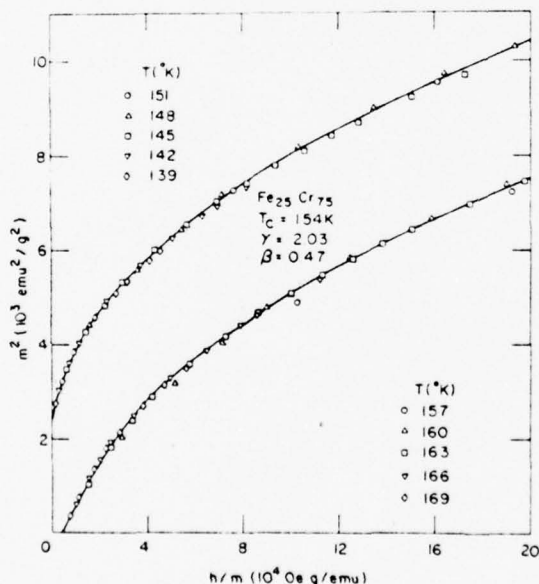


Fig. 1. Plot of some normalized isotherms (see text) near T_c for an Fe₂₅Cr₇₅ sample.

obtained in this way are also listed in table I. Because of uncertainties in the extrapolation procedures and the theoretical estimate of $\mu^* h_0 / kT_c$, the values of μ^* and c^* should be considered approximate. However, a general trend appears in that, as the critical concentration is approached from the ferromagnetic side, the giant-moment clusters become larger in magnitude and smaller in concentration.

From these results, we conclude that the Curie-point transition in weakly ferromagnetic Fe-Cr alloys involves the magnetic order-disorder of a dilute concentration of giant-moment clusters. Moreover, the critical exponents that characterize this transition have anomalous values similar to those of other giant-moment alloy systems.

References

- [1] M. Fallot, *Ann. Phys.* 6 (1936) 305.
- [2] A.T. Aldred, *Phys. Rev.* B14 (1976) 219.
- [3] A.T. Aldred, B.D. Rainford, J.S. Kouvel and T.J. Hicks, *Phys. Rev.* B14 (1976) 228.
- [4] T.J. Hicks, B.D. Rainford, J.S. Kouvel, G.G. Low and J.B. Comly, *Phys. Rev. Lett.* 22 (1969) 531.
- [5] Y. Ishikawa, R. Tournier and J. Fillippi, *J. Phys. Chem. Solids* 26 (1965) 1727.
- [6] R.D. Shull and P.A. Beck, *AIP Conf. Proc.* 24 (1975) 95.
- [7] B. Loegel, *J. Phys.* F5 (1975) 497.
- [8] B. Loegel, J.M. Friedt and R. Poinso, *J. Phys.* F5 (1975) L54.
- [9] J.S. Kouvel and J.B. Comly, in *Critical Phenomena in Alloys, Magnets, and Superconductors*, R.E. Mills, E. Ascher and R.I. Jaffee, eds. (McGraw-Hill, New York, 1971).
- [10] A.T. Aldred, B.D. Dunlap, D.J. Lam and I. Nowik, *Phys. Rev.* B10 (1974) 1011.
- [11] J.S. Kouvel and J.B. Comly, *Phys. Rev. Lett.* 20 (1968) 1237.
- [12] W.C. Mueller and J.S. Kouvel, *Solid State Commun.* 15 (1974) 441.

THE MICTOMAGNETIC TRANSITION IN Cu-Mn*

H. Claus and J.S. Kouvel

Department of Physics, University of Illinois, Chicago, IL 60680, U.S.A.

(Received 24 July 1975 by A.G. Chynoweth)

The isothermal magnetization processes in the alloy $\text{Cu}_{81}\text{Mn}_{19}$ are found to undergo a qualitative change, involving the sudden appearance of magnetic hysteresis, at the temperature ($\sim 85^\circ\text{K}$) at which the initial susceptibility has a sharp maximum.

THE COMPLEX magnetic properties of Cu-Mn and certain other transition-group alloy systems have been attributed to a correspondingly complex magnetic state known variously as a mictomagnetic or spin-glass state.¹ Whereas the mictomagnetic picture for these atomically disordered alloys stresses an inhomogeneous coexistence of ferromagnetic and antiferromagnetic local spin alignments, the spin-glass picture emphasizes a nearly random distribution of atomic spin orientations. At low temperatures, both pictures allow for strong local anisotropy forces which "freeze in" a static spin configuration with no long-range magnetic order.

The important role in Cu-Mn of some type of local magnetic anisotropy was first seen in the unusual displaced hysteresis loops which result from cooling the alloys in a magnetic field.² Furthermore, when an alloy in this metastable field-cooled state is warmed up, there is an enormous increase in magnetic hysteresis losses as the measured loops gradually lose their asymmetry.² In apparent contrast with this gradual process, the initial (low-field) susceptibility of Cu-Mn was recently found to exhibit a cusp-like maximum.³ For a given alloy composition, this sharp phenomenon occurs at essentially the temperature at which the effects produced by field-cooling disappear.^{2,3} Although the sharp susceptibility peak may

suggest a Néel-point transition to an antiferromagnetically ordered state, the neutron diffraction evidence for any type of *long-range* magnetic order in Cu-Mn is quite negative.⁴ The current interpretation of this sharp behavior is that it marks the rapid freezing in of a complex glass-like spin configuration of the type mentioned above. However, this interpretation is not definitive, and many interrelated properties need to be explored before the magnetic states of Cu-Mn can be properly understood.

In this paper, we report on a magnetization study of a concentrated Cu-Mn alloy. The isothermal magnetization processes are found to undergo a qualitative change, involving the sudden appearance of magnetic hysteresis, at the temperature at which the initial susceptibility has a sharp maximum. Thus, the sharp susceptibility peak is seen as one of several manifestations of an unusual magnetic transition.

For this study, a piece was taken from an alloy ingot (prepared by induction-melting under argon) of nominal atomic composition $\text{Cu}_{81}\text{Mn}_{19}$, and was cold-worked by hammering. A cylindrical sample was cut from this ingot piece, annealed for three days at 800°C and water-quenched, and then aged by slow-cooling from 350°C to room temperature at a rate of $10^\circ\text{C}/\text{day}$. The magnetization measurements were made with a vibrating-sample magnetometer at temperatures down to 4.2°K and in fields up to 56 kOe .

* This work was supported in part by the National Science Foundation and the Office of Naval Research.

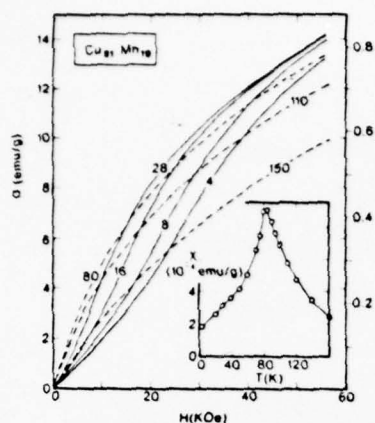


FIG. 1. Magnetization vs field curves for $\text{Cu}_{81}\text{Mn}_{19}$ cooled to various temperatures (in $^{\circ}\text{K}$) in zero field; each curve was measured isothermally with increasing field. Insert: initial susceptibility vs temperature as determined from the initial slopes of the various isotherms.

In the first set of experiments, the sample was cooled in zero field from above $\sim 100^{\circ}\text{K}$ to various temperatures down to 4.2°K . This procedure ensured that at each temperature of measurement the sample started in a magnetically virgin state with zero remanence. Isothermal magnetization curves were then obtained with increasing fields up to 56 kOe; a typical selection of them are shown in Fig. 1. The initial slopes of these curves, corresponding to the initial susceptibilities, are plotted vs temperatures in the insert of the figure. The susceptibilities clearly describe a sharp maximum at $\sim 85^{\circ}\text{K}$, in qualitative agreement with previous a.c. measurements.³ It should also be noted that at this same temperature the magnetization curves as a whole undergo a qualitative change in shape. The curves above 85°K are uniformly concave-downward, while the curves below 85°K start with a positive curvature and become concave-downward only at higher fields. With decreasing temperature, the inflection point of the latter curves moves steadily upward in field, reaching ~ 25 kOe at 4.2°K .

In the second set of experiments, we investigated the possibility that the anomalous magnetic behavior below 85°K may be irreversible. The alloy sample was cooled in zero field to 4.2°K , its field raised to some value H' , and its magnetization measured as the field was reduced from H' to zero. This

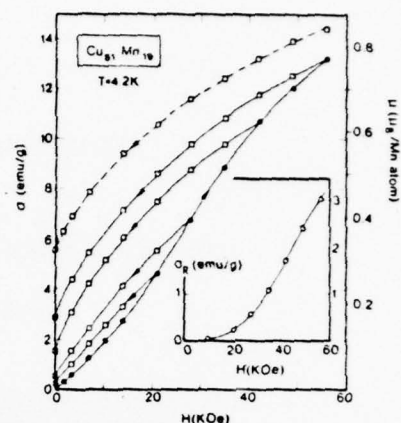


FIG. 2. Magnetization vs field for $\text{Cu}_{81}\text{Mn}_{19}$ at 4.2°K . Solid curves measured after cooling in zero field, raising field to some value H' (each represented by closed circle), then reducing field to zero. Dashed curve measured after cooling in 56 kOe field. Insert: remanent magnetization vs H' at 4.2°K .

entire procedure was repeated for different values of H' , and our results are illustrated by the solid curves in Fig. 2. Hysteresis obviously does occur and gives rise to an isothermal remanence σ_R . However, this effect remains extremely small until H' is raised out of the initial linear region of the virgin magnetization curve. The plot of σ_R vs H' in the insert of Fig. 2 shows that the behavior is reversible below a threshold H' value of ~ 15 kOe. At higher values of H' , σ_R rises very rapidly, although its rate of rise is decreasing at our largest H' value of 56 kOe, which suggest an approach to saturation. The dashed curve in Fig. 2, measured after cooling to 4.2°K in 56 kOe, gives a remanence value of nearly 6 emu/g, which is probably also the saturation level of the isothermal remanence at 4.2°K . The measurements of isothermal remanence were also carried out at higher temperatures, and it was found that its threshold behavior and its approach to saturation occur at H' values that decrease to zero — and the remanences themselves decrease to zero — as the temperature approaches 85°K . Above this temperature, the magnetization is reversible at all fields.

Thus, the temperature ($T_m \approx 85^{\circ}\text{K}$) of the low-field susceptibility peak marks a transition in the nature of the isothermal magnetization processes. When cooled to below T_m in zero field, the alloy appears to sink into a low-magnetization state, from

which it can be lifted isothermally but irreversibly by the application of a field above a certain threshold value. All aspects of this behavior are consistent with the onset of local anisotropy at T_m and its gradual strengthening at lower temperatures. However, anisotropy cannot be solely responsible for the low-magnetization state if substantial exchange forces are present, which is bound to be the case especially in this concentrated alloy. If the mictomagnetic picture is valid, exchange interactions in the alloy produce an inhomogeneous magnetic state in which all the Mn moments tend to cancel out vectorially. An interesting question arises at this juncture: does the mictomagnetic state form simultaneously with the onset of

anisotropy at T_m or is it produced at some higher temperature by isotropic exchange and is then simply frozen in by the anisotropy at and below T_m ? The latter possibility appears to be supported by recent neutron scattering experiments on a Cu-Mn alloy of similar composition, which indicate that the magnetic correlations in the alloy are essentially unchanged from 4.2 up to 78°K.⁵ Further experiments are required, however, before this question can be answered (or even asked) unambiguously. Moreover, the same question probably also applies to other spin-glass alloy systems such as Au-Fe, whose isothermal remanence is found to disappear at the temperature of the low-field susceptibility peak.⁶

REFERENCES

1. This subject was recently reviewed by MYDOSHI J.A. in *Magnetism and Magnetic Materials* - 1974, p. 131. AIP Conf. Proc., No. 24, (1975).
2. KOUVEL J.S., *J. Phys. Chem Solids* 21, 57 (1961); *ibid.* 24, 795 (1963). For a recent review of these and related properties, see BECK P.A. In *Magnetism in Alloys* (Edited by BECK P.A. & WABER J.T.) p. 211. TMS-AIME, NY (1972).
3. CANNELLA V. & MYDOSHI J.A., *Magnetism and Magnetic Materials* - 1973, p. 651. AIP Conf. Proc., No. 18 (1974).
4. AHMED N. & HICKS T.J., *Solid State Commun.* 15, 415 (1974).
5. FELCHER G.P., WERNER S.A., MAJEWSKI R.E. & KOUVEL J.S., *Magnetism and Magnetic Materials* - 1974, p. 427. AIP Conf. Proc., No. 24 (1975).
6. THOLENCE J.L. & TOURNIER R., *J. Phys.* 35, C4-229 (1974).

Biquadratic exchange coupling and the magnetic properties of PrAg[†]

T. O. Brun, J. S. Kouvel,* and G. H. Lander

Argonne National Laboratory, Argonne, Illinois 60439

(Received 15 January 1976)

Bulk magnetic and neutron diffraction studies show that the cubic (CsCl-type) compound PrAg becomes antiferromagnetic at $T_N \approx 11^\circ\text{K}$, below which it undergoes a spin-flop transition at a critical field H_c of ~ 5 kOe. However, the temperature dependence of the initial susceptibility below T_N and the field dependence of the magnetization M above H_c are both anomalous. The measured M vs H curves for PrAg above T_N and those for the related pseudobinary $\text{Pr}_{0.5}\text{La}_{0.5}\text{Ag}$ (which remains paramagnetic down to 4.2°K) are tested against the isotherms of M vs effective field calculated for the crystal-field states of Pr^{3+} in these compounds. This analysis reveals that the net exchange field H_{exch} on a Pr atom in either compound does not vary linearly with M but also contains a substantial negative term in M^3 . It is shown that this higher-order $H_{\text{exch}}(M)$ dependence can be generated by a positive biquadratic exchange term in the spin Hamiltonian of the paramagnetic system. Moreover, when the same biquadratic exchange term is included in a two-sublattice model for the ordered magnetic state, a consistent explanation is obtained for the anomalous properties of PrAg below T_N . Possible mechanisms for the origin of biquadratic exchange in these materials are discussed.

I. INTRODUCTION

The cubic (CsCl-type) intermetallic compound PrAg, according to recent neutron-diffraction work,¹ orders antiferromagnetically at $\sim 14^\circ\text{K}$. In its collinear two-sublattice structure, the ordered Pr moments ($\sim 2.1\mu_B$) in adjacent ferromagnetic (110) planes are antiparallel and lie within (001) planes. This antiferromagnetic structure is identical, except for the orientation of the moment axis, to the $(\pi\pi 0)$ structures deduced from similar studies of NdAg,² TbAg,³ DyAg,⁴ HoAg,⁵ and ErAg,⁶ the latter two also exhibiting modulated variations. However, in two separate reports^{7,8} on the bulk magnetic properties of this family of isomorphous rare-earth-silver compounds, it is claimed that in the case of PrAg the field and temperature dependences of the magnetization are indicative of ferromagnetic rather than antiferromagnetic ordering.

This apparent inconsistency prompted us to undertake a more detailed investigation of the bulk magnetic properties of PrAg. At low fields (H), our magnetization (M) versus temperature data for a polycrystalline sample show a peak at $\sim 11^\circ\text{K}$, clearly indicating the onset of antiferromagnetism, although there is also an anomalous upturn in M at lower temperatures. Furthermore, the measured M vs H curves below 11°K exhibit an inflection point at a critical field (H_c), which suggests a spin-flop transition to a canted state. But again the total behavior is anomalous, in that the M vs H curves at fields well above H_c are not linear but distinctly concave downward. This high-field behavior, by itself, would appear to agree

with the previous reports^{7,8} that PrAg is ferromagnetic. However, from subsequent neutron-diffraction experiments, we have found that PrAg does indeed undergo a field-induced transition to a canted state. The nonlinear M vs H behavior of the spin-flopped state thus remains as a real anomaly. Our experimental results for PrAg, which were recently reported in brief,⁹ as well as those for the related pseudobinary compound $\text{Pr}_{0.5}\text{La}_{0.5}\text{Ag}$ (where the La substitution suppresses any magnetic ordering down to 4.2°K , at least), are fully described in Sec. II of this paper.

Theoretical analyses of our results are presented in Sec. III. Starting with the crystal-field states for Pr^{3+} in PrAg (where the ground state is a magnetic Γ_3 triplet), as determined recently from inelastic-neutron-scattering measurements,¹⁰ we calculate various isotherms of M vs H_{eff} , the total effective field. Comparing our low-temperature paramagnetic M vs H data against the corresponding M vs H_{eff} isotherms, we find that in both PrAg and $\text{Pr}_{0.5}\text{La}_{0.5}\text{Ag}$ the net exchange field ($H_{\text{exch}} = H_{\text{eff}} - H$) does not depend simply linearly on M , but contains a substantial negative term in M^3 . We proceed to show that a higher-order $H_{\text{exch}}(M)$ dependence of this kind can be generated by a biquadratic exchange term in the effective spin Hamiltonian of the paramagnetic system. Furthermore, by the inclusion of the same biquadratic exchange term in a two-sublattice model for the antiferromagnetic state, a consistent semiquantitative explanation is obtained for the various anomalous magnetic properties of PrAg below its Néel point.

In Sec. IV several possible mechanisms for the

origin of biquadratic exchange in PrAg and $\text{Pr}_{0.5}\text{La}_{0.5}\text{Ag}$ are discussed with reference to previous related work on rare-earth materials.

II. EXPERIMENTAL RESULTS

A. Magnetization and susceptibility

For our magnetization measurements, polycrystalline samples of PrAg and $\text{Pr}_{0.5}\text{La}_{0.5}\text{Ag}$ in the form of thin platelets weighing 0.13 and 0.11 g, respectively, were cut from arc-melted buttons and annealed at 700°C for 4 h under argon. The same annealing treatment previously given to larger samples taken from the same buttons for neutron-diffraction study was found to produce a single cubic phase of appropriate lattice spacing.¹ The sample preparation and their subsequent storage and measurement were all carried out in an inert atmosphere to avoid excessive oxidation. The sample magnetizations were measured in a vibrating-sample magnetometer in fields up to 56 kOe at temperatures down to 4.2°K.

The magnetization (M , in μ_B per Pr atom) of PrAg is plotted in Fig. 1(a) against temperature for various values of the applied field (H); demagnetization corrections to H were negligible. Included is the remanent magnetization for H reduced from 56 kOe to zero, which is measurable at low temperatures but extremely small ($\leq 0.02\mu_B/\text{Pr}$) relative to the magnetizations attained in moderate fields. A more prominent feature of the curves for low fields (1 and 3.5 kOe) is the peak at $\sim 11^\circ\text{K}$, which is typical of a polycrystalline antiferromagnet at its Néel point (T_N). However, in that regard, the rise of these curves at lower temperatures, corresponding to a rise in the initial susceptibility, is quite anomalous. At higher fields, the peak in the curves is replaced by an abrupt change of slope, which occurs at a slowly decreasing temperature with increasing field; below this temperature, the magnetization at high fields is almost constant. This high-field behavior suggests that the material has undergone a spin-flop transition to a canted state.

Some of the same data on PrAg are plotted in Fig. 1(b) as isotherms of M vs H . The curves for 12 and 14°K, in their concave-downward curvature at all fields, are characteristic of all our data above T_N . Contrastingly, the curves for 4.2 and 10°K both exhibit an inflection point at ~ 4.5 kOe, which may be taken as the average critical field (H_c) for the spin-flop transition in this polycrystalline sample. However, above H_c , the magnetization at 4.2°K does not show the linear increase with field that is normally expected of a spin-flopped state at low temperatures. Instead, M appears to vary as the cube root of H . This unusual

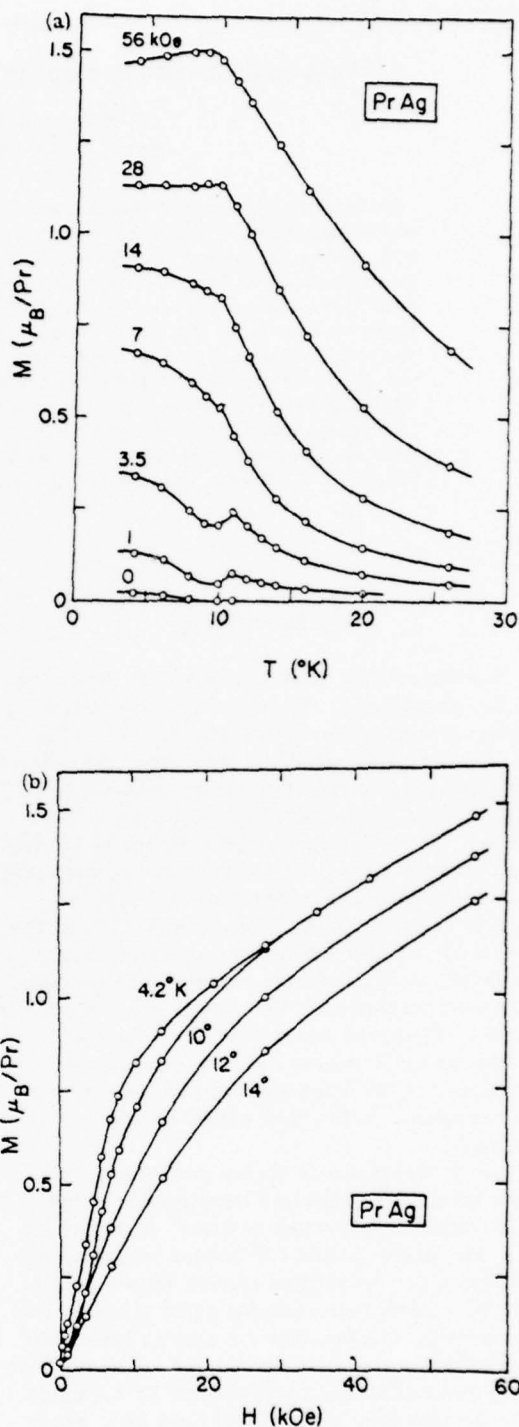


FIG. 1. Magnetization of PrAg, in μ_B per Pr atom, as (a) a function of temperature at various fields and (b) a function of field at various temperatures.

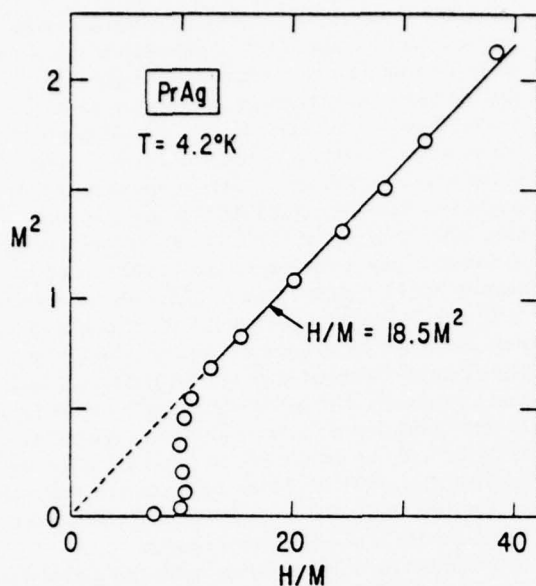


FIG. 2. M^2 vs H/M for PrAg at 4.2°K, where M is the magnetization (μ_B per Pr atom) and H the magnetic field (kOe).

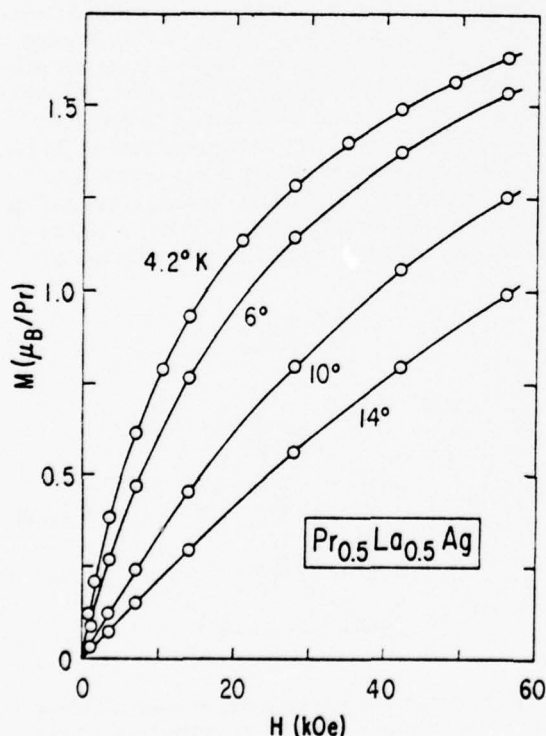


FIG. 3. Magnetization of $\text{Pr}_{0.5}\text{La}_{0.5}\text{Ag}$, in μ_B per Pr atom, as a function of field at various temperatures.

cube-root dependence is brought out more clearly in Fig. 2, where the same data are plotted as M^2 vs H/M . Above a threshold field, the data in this plot follow close to a straight line that extrapolates back to the origin. Nevertheless, despite its anomalous appearance, this high-field behavior is associated with a canted magnetic state, as our neutron-diffraction study of PrAg in high fields (described below) has demonstrated.

Our low-temperature magnetization data on $\text{Pr}_{0.5}\text{La}_{0.5}\text{Ag}$ are plotted as isotherms of M vs H in Fig. 3. From the linearity of these curves at low fields and the smooth monotonic changes with field and temperature, it is evident that this material remains paramagnetic down to 4.2°K. It has therefore allowed us the advantage of extending our analysis of the paramagnetic state (Sec. IIIA) to temperatures well below the T_N of PrAg and, thus, to higher levels of induced moment per Pr atom.

In Fig. 4, our low-field results for PrAg and $\text{Pr}_{0.5}\text{La}_{0.5}\text{Ag}$ are exhibited as plots of the inverse initial susceptibility (χ_0^{-1}) versus temperature (T). The two curves are essentially identical in shape with a constant vertical separation that presumably arises from a difference in the net exchange cou-

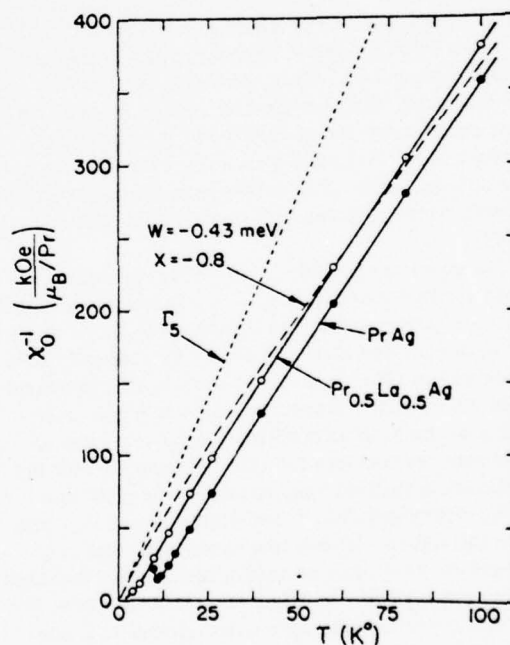


FIG. 4. Inverse initial susceptibility versus temperature for PrAg and $\text{Pr}_{0.5}\text{La}_{0.5}\text{Ag}$. The dashed curve was calculated for the crystal-field parameters, $W = -0.43$ meV, $x = -0.8$; the dotted curve represents the Γ_5 ground state alone.

pling. They both decrease in slope with increasing T up to $\sim 25^\circ\text{K}$, above which they are linear and obey the Curie-Weiss law, $\chi_0^{-1} = (T - \Theta)/C_{CW}$, with $C_{CW} = 0.265 \text{ K } \mu_B/\text{kOe}$, corresponding to an effective paramagnetic moment per Pr atom (μ_p) of $3.44 \mu_B$. The values of Θ are 6°K for PrAg and 0°K for $\text{Pr}_{0.5}\text{La}_{0.5}\text{Ag}$. Our results for PrAg agree quite closely with those of Walline and Wallace⁷ ($\mu_p = 3.44 \mu_B$, $\Theta = 2^\circ\text{K}$), but less closely with those of Pierre and Pauthenet⁸ ($\mu_p = 2.97 \mu_B$, $\Theta = 14^\circ\text{K}$). The values of μ_p should be compared with the theoretical value of $3.58 \mu_B$ for the free Pr^{3+} ion, which is represented in Fig. 4 by the high-temperature slope of the dashed curve calculated for the crystal-field parameters to be discussed later. The discrepancy with the high-temperature slopes of our experimental curves conceivably arises from changes in the exchange coupling produced by thermal lattice expansion.

B. Neutron diffraction

To investigate specifically the possibility that PrAg undergoes a field induced spin-flop transition, we carried out an elastic-neutron-diffraction study of this material at the CP-5 reactor of the ANL. The sample was a 2-g compact of powder that had been used for previous neutron-diffraction work.¹ All the measurements were made with the sample at $\sim 5^\circ\text{K}$ and in a magnetic field of up to 60 kOe applied perpendicular to the scattering vector (\vec{k}). Thus, for each (hkl) reflection investigated, the only crystallites of the sample that contributed to the measured intensity were those whose (hkl) planes contained the direction of the applied field. The reflections studied were the superlattice $(\frac{1}{2}\frac{1}{2}0)$ and $(\frac{1}{2}\frac{1}{2}1)$ and the fundamental (100) .

The geometry for the $(\frac{1}{2}\frac{1}{2}0)$ reflection measurement is illustrated in Fig. 5. A scattering crystallite is represented by its chemical unit cell and the Pr moments are shown in the $(\pi\pi 0)$ configuration, lying within (001) planes, as determined previously in zero field.¹ Moreover, although the orientation of the spin axis within the (001) planes is unknown, we assume for this illustration that the magnetocrystalline easy axes are the $[110]$ and $[\bar{1}\bar{1}0]$, corresponding respectively to cases A and B in the figure. These two cases will thus represent the two types of antiferromagnetic domains in the crystallite. In this zero-field situation, the B domains with their spin axes normal to \vec{k} contribute fully to the measured $(\frac{1}{2}\frac{1}{2}0)$ reflection, whereas the A domains with their spin axes parallel to \vec{k} make zero contribution. When the external field (\vec{H}) is applied, it lies in some direction within the (110) plane of the crystallite, as

indicated in the figure. The field therefore has a component parallel to the spin axes of the B domains, which favors a reorientation (or flop) of the moments into the plane perpendicular to \vec{H} . Under these circumstances, the spin flop would cause some reduction of the observed intensity. If there is, in addition, a strong anisotropy that holds the moments in the (001) plane, the spin flop induced by H would effectively transform the B domains into A domains, and the observed intensity would reduce to zero. Since the component of \vec{H} parallel to the spin axes of the B domains will differ for different crystallites, the latter process can be expected to proceed rapidly and then more gradually throughout the sample as the field is increased beyond a critical value. A similar reduction can be predicted for the $(\frac{1}{2}\frac{1}{2}0)$ intensity with increasing field if the easy axes are taken to be the $[100]$ and $[010]$ and, again, if the anisotropy out of the (001) plane is very strong.

The intensities of the three measured reflections at various fields are shown in Fig. 6. For the $(\frac{1}{2}\frac{1}{2}0)$ reflection with increasing field, the intensity drops rapidly between ~ 4 and 6 kOe and then diminishes more slowly until it has vanished at ~ 60 kOe. Qualitatively, this behavior is entirely consistent with that described above for the occurrence of a spin-flop transition. Moreover, the critical field for this transition appears to be ~ 5 kOe, in good agreement with the H_c value derived from our magnetization data. For the $(\frac{1}{2}\frac{1}{2}1)$ reflection, the measured intensity shows little change until it decreases slowly with increasing field above ~ 20 kOe. In this case, if the spin axis of each crystallite stays within the (001) plane following the spin-flop transition, as described above, there should be almost no change of intensity. The intensity de-

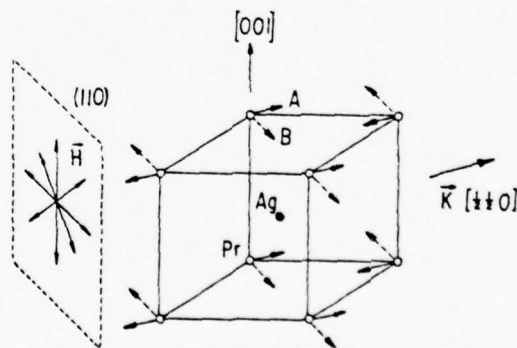


FIG. 5. Schematic representation of neutron-diffraction measurements of the $(\frac{1}{2}\frac{1}{2}0)$ reflection from a PrAg crystallite in an external field in the (110) plane. The solid and dashed spin vectors in the (001) plane correspond to two types of antiferromagnetic domains.

crease seen at higher fields can be readily ascribed to an increased canting of the moments and to the consequent reduction of the antiferromagnetic spin component, the $(\frac{1}{2}\frac{1}{2}1)$ intensity depending on the square of this component. Hence, the fact that the $(\frac{1}{2}\frac{1}{2}1)$ intensity is still appreciable at 60 kOe indicates that the spin canting persists up to much higher fields before ferromagnetic alignment is ultimately achieved. The intensity of the (100) reflection, which rises monotonically with increasing field, contains a small field-independent nuclear part plus a magnetic part that varies as the square of the ferromagnetic spin component. In Fig. 6, we have allowed for the nuclear intensity and fitted the data points with a curve derived quantitatively from the M vs H curve for 4.2 °K in Fig. 1(b). The fit is clearly excellent. In essence, this latter result confirms the cube-root M vs H behavior of PrAg shown in Fig. 2. It thus establishes, when combined with our results for the $(\frac{1}{2}\frac{1}{2}0)$ and $(\frac{1}{2}\frac{1}{2}1)$ reflections, that this unusual behavior is exhibited when the material is in a canted magnetic state following a spin-flop transition.

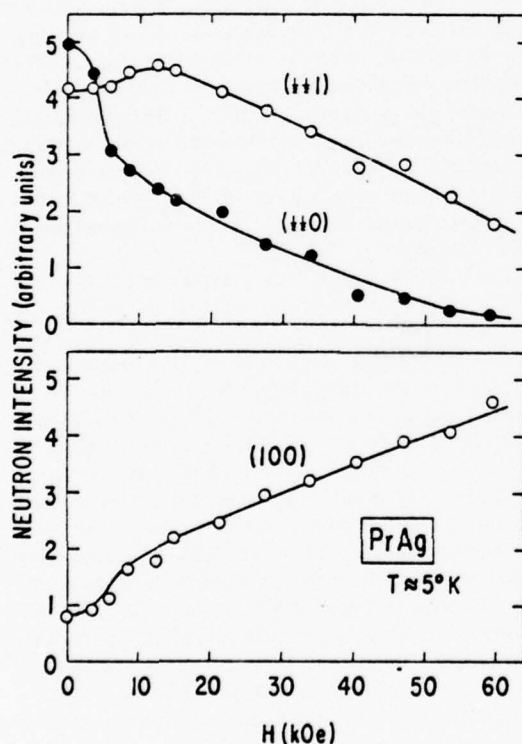


FIG. 6. Neutron intensities of various reflections from PrAg at $\sim 5^\circ\text{K}$, as functions of the applied field normal to the scattering vector. The (100) curve was derived from bulk magnetization data.

III. THEORETICAL ANALYSES

A. Paramagnetic state

Inelastic-neutron-scattering work¹⁰ has recently established the crystal-field level scheme for the Pr^{3+} ion in both PrAg and $\text{Pr}_{0.5}\text{La}_{0.5}\text{Ag}$. As shown in Fig. 7, the ground-state multiplet of the free ion ($J=4$, $g=\frac{4}{3}$) is split by the cubic crystal field into four levels which, with increasing energy, are a Γ_5 triplet, a Γ_3 doublet, a Γ_4 triplet, and a Γ_1 singlet. In the notation of Lea *et al.*,¹¹ the sequence and separation of these levels is given by $W = -0.43$ meV, $x = -0.8$. This sequence is the reverse of that for the cubic (NaCl-type) Pr chalcogenides and pnictides, which are singlet-ground-state systems.^{12,13}

The ground state of PrAg and $\text{Pr}_{0.5}\text{La}_{0.5}\text{Ag}$ being a magnetic triplet, it follows that a Pr atom (acting as a tripositive ion) in these compounds will be increasingly polarizable by an effective field (H_{eff}) as the temperature decreases to zero. In fact, at $T=0$, the initial effective susceptibility $(\chi_{\text{eff}})_0 = (M/H_{\text{eff}})_0$ will diverge. This is shown in Fig. 4, where the calculated dashed curve of $(\chi_{\text{eff}})_0^{-1}$ vs T emerges from the origin. Moreover, the slope of this curve at $T=0$ is determined solely by the Γ_5 ground-state triplet and is represented by the dotted line in Fig. 4. Its value

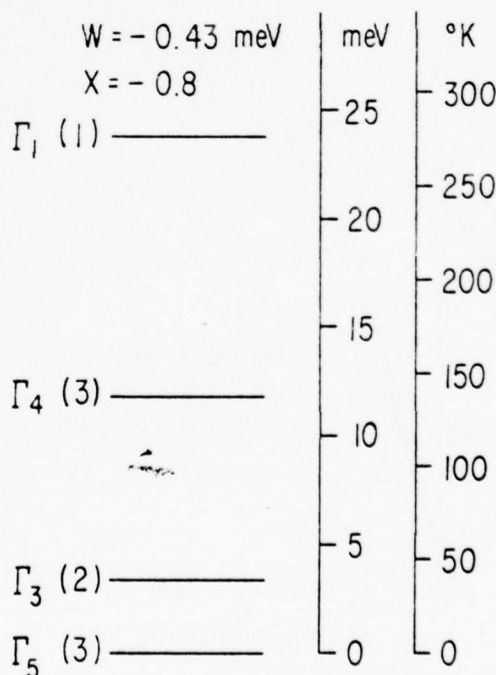


FIG. 7. Crystal-field energy levels for Pr^{3+} in PrAg and $\text{Pr}_{0.5}\text{La}_{0.5}\text{Ag}$.

corresponds to a paramagnetic moment (μ_B) of $2.82\mu_B$, since the Γ_3 triplet alone constitutes a system of pseudospin $S=1$, $g=2$. Note that the calculated dashed curve in Fig. 4, in its decrease of slope with increasing temperature, matches the shape of the experimental curves up to $\sim 40^\circ\text{K}$; the discrepancy at higher temperature was commented on earlier.

As standards of comparison for the entire paramagnetic M vs H behavior of the two compounds (not merely their initial susceptibilities), we calculated various isotherms of M vs H_{eff} on the basis of the crystal-field levels shown in Fig. 7. The effective field H_{eff} was taken to be parallel, in turn, to each of the principal crystallographic axes. The results of these calculations are represented conveniently as isotherms of M vs H_{eff}/T in Fig. 8. The curve labeled 0°K corresponds to the isotropic response of the Γ_3 ground-state triplet alone; it is a Brillouin function and saturates at $2\mu_B$. The curve labeled ∞ gives the isotropic high-temperature response of all nine states; its saturation level is $3.2\mu_B$. These two extreme curves bracket the curves for all intermediate (normal) temperatures for all directions and

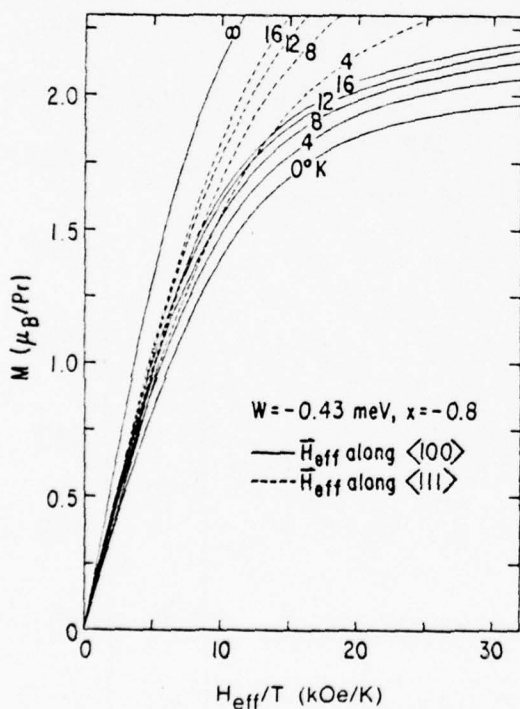


FIG. 8. Magnetization (in μ_B per Pr atom) vs H_{eff}/T calculated for PrAg and $\text{Pr}_{0.5}\text{La}_{0.5}\text{Ag}$ at various temperatures (T , in $^\circ\text{K}$) for effective fields (H_{eff} , in kOe) parallel to $\langle 100 \rangle$ or $\langle 111 \rangle$.

strengths of \vec{H}_{eff} . At each temperature, the initial slopes of the curves are the same for all directions of \vec{H}_{eff} , i.e., the initial susceptibilities are isotropic, as required by the cubic symmetry of the structure. However, with increasing field, the curves for \vec{H}_{eff} parallel to $\langle 111 \rangle$ diverge from and lie consistently above the corresponding isotherms for \vec{H}_{eff} along $\langle 100 \rangle$; the curves for \vec{H}_{eff} along $\langle 110 \rangle$ are intermediate and are not shown in Fig. 8. At the highest magnetizations ($\sim 1.5\mu_B/\text{Pr}$) reached by our paramagnetic data for the two compounds, the anisotropy of these curves is fairly small; for our data analysis, we specifically used the curves for \vec{H}_{eff} along $\langle 100 \rangle$.

In the analysis of our paramagnetic data for PrAg and $\text{Pr}_{0.5}\text{La}_{0.5}\text{Ag}$, the net effect of all the exchange interactions on each Pr atom is considered to be representable by an exchange field \vec{H}_{exch} which is collinear with the externally applied field \vec{H} . With the direction of \vec{H} as reference, the magnitude of the total effective field is given by $H_{\text{eff}} = H_{\text{exch}} + H$, where H_{exch} may be positive or negative. Hence, within this effective-field approximation, we can consider an experimental $M(H, T)$ data point, refer to the appropriate isotherm among the calculated curves represented in Fig. 8 and find the value of H_{eff} corresponding to the measured M , and thus determine the exchange field, $H_{\text{exch}} = H_{\text{eff}} - H$, for the particular M and T . This procedure was followed with all our low-temperature paramagnetic data on the two compounds, including the data on PrAg for $H \geq 7$ kOe at 10°K , which from Fig. 1(a) appear to be just within the paramagnetic regime.

The results of this data analysis are presented in Fig. 9(a) as isothermal plots of M^2 vs H_{exch}/M . If simple mean-field theory is valid and H_{exch} is proportional to M (and not otherwise dependent on T), the reduced data points in this form of representation can be expected to follow a single vertical straight line for each material. Clearly, the results in Fig. 9(a) do not bear out this expectation. Although the isotherms for each compound do cluster fairly closely together and they do form reasonably straight lines, the lines have a pronounced tilt corresponding to decreases of H_{exch}/M with increasing M^2 . At high M^2 , the isotherms appear to be deviating from linearity towards even smaller values of H_{exch}/M . In fact, in the case of $\text{Pr}_{0.5}\text{La}_{0.5}\text{Ag}$ at 4.2°K , H_{exch}/M ultimately changes sign from positive to negative—which underscores the enormous magnitude of this phenomenon. These results can be expressed in summary as follows:

$$H_{\text{exch}}/M = \lambda + \lambda' M^2 + \dots \quad (1)$$

or, equivalently,

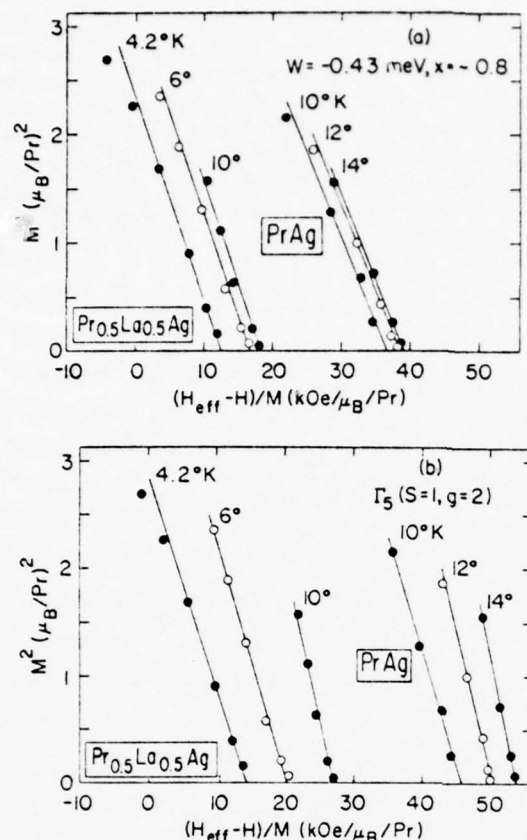


FIG. 9. Isotherms of M^2 vs $(H_{\text{eff}} - H)/M$ derived from data on PrAg and $\text{Pr}_{0.5}\text{La}_{0.5}\text{Ag}$ on the basis of (a) the crystal-field parameters, $W = -0.43$ meV, $x = -0.8$, and (b) the Γ_5 ground state alone.

$$H_{\text{exch}} = \lambda M + \lambda' M^3 + \dots \quad (1')$$

where λ is the usual exchange coefficient and λ' is the coefficient associated with some higher-order process. Terms of still higher order in M are implied in these expressions in order to

allow for the nonlinearity of the isotherms in Fig. 9(a) at high M^2 ; they should be such that odd symmetry between H_{exch} and M is preserved. The values of λ and λ' derived from the data in Fig. 9(a) are listed in Table I. For each compound, the two coefficients show little variation with temperature.

For comparison, we carried out an analogous treatment of the same data, using exclusively the $M(H_{\text{eff}}, T)$ characteristics of the Γ_5 ground-state triplet (i.e., the 0 K curve in Fig. 8). The results for M^2 vs H_{exch}/M are plotted in Fig. 9(b). The isotherms again form lines of decidedly negative slope. However, their values at zero M and their slopes, corresponding, respectively, to λ and $(\lambda')^{-1}$ in Eq. (1), vary much more with temperature than those of their counterparts in Fig. 9(a). The λ and λ' values are listed in Table I and bear out this comparison. Thus, if the constancy of λ and λ' with temperature is a meaningful criterion, it appears distinctly preferable in this type of analysis to use the $M(H_{\text{eff}}, T)$ curves computed for the full spectrum of crystal-field levels rather than the curves for the Γ_5 triplet alone. Nevertheless, since the results in Fig. 9(a) are quite similar in basic character to those in Fig. 9(b), it is not unreasonable at these low temperatures to consider only the ground-state triplet and, in doing so, simplify enormously any theoretical investigation of the magnetic properties of the two compounds.

The higher-order dependence of H_{exch} on M , as revealed by our data analysis, presumably arises from an equivalently higher-order component of the effective exchange coupling. Specifically, the M^3 term in Eq. (1') suggests that the spin Hamiltonian for these materials contains an exchange term that is quartic in the spin variables. The simplest of such terms has the biquadratic form $(\vec{S}_i \cdot \vec{S}_j)^2$ for two interacting spins. In keeping with the fact that all our experimental data are for polycrystalline samples, we will restrict our

TABLE I. Bilinear and biquadratic exchange coefficients.

T (°K)	PrAg			
	$W = -0.43$ meV, $x = -0.8$		Γ_5 ($S=1, g=2$)	
	λ (kOe/ μ_B)	λ' (kOe/ μ_B^3)	λ (kOe/ μ_B)	λ' (kOe/ μ_B^3)
10	36.6	-6.3	45.6	-4.6
12	38.5	-6.4	50.3	-3.7
14	39.1	-6.4	53.6	-3.2
Pr _{0.5} La _{0.5} Ag				
4	12.4	-5.3	14.4	-5.1
6	16.6	-5.3	20.1	-4.5
10	18.2	-5.3	27.0	-3.5

considerations to this isotropic biquadratic term plus an isotropic bilinear exchange term of the usual form $\tilde{S}_i \cdot \tilde{S}_j$. Moreover, in the approximation that PrAg and $\text{Pr}_{0.5}\text{La}_{0.5}\text{Ag}$ are characterized adequately by their crystal-field ground-state triplet, they will be regarded as simple isotropic systems of effective spin $S=1$ and $g=2$. Extending from this particular case to any S , we express the quantum-mechanical Hamiltonian of the i th spin of the system as

$$\mathcal{H}_i = -g\mu_B \tilde{H} \cdot \tilde{S}_i - \sum_{j \neq i} [J_{ij} \tilde{S}_i \cdot \tilde{S}_j + J'_{ij} (\tilde{S}_i \cdot \tilde{S}_j)^2], \quad (2)$$

where \tilde{H} is the external field, and J_{ij} and J'_{ij} are, respectively, the coefficients for the bilinear and biquadratic exchange interactions with all other (j)th spins.

The mean-field approximation to the spin Hamiltonian of Eq. (2) can be written as

$$\mathcal{H}_i = - \sum_{\alpha} \left(\sum_{\beta} (g\mu_B H_{\alpha} + J_{i\alpha} \langle S_{i\alpha} \rangle) S_{i\alpha} + \sum_{\alpha, \beta} J'_{i\alpha} \langle S_{i\alpha} S_{i\beta} \rangle S_{i\alpha} S_{i\beta} \right), \quad (2')$$

where α and β represent Cartesian coordinates (x, y, z) permuted in the summations, and $\langle \rangle$ corresponds to a thermal average. This mean-field Hamiltonian has been treated previously by Lines and Jones¹⁴ for the case of a collinear anti-ferromagnet in zero \tilde{H} . Our problem here being the paramagnetic state in nonzero \tilde{H} , we will apply the same treatment but with \tilde{H} placed along the z axis and with the j summations making no distinction between magnetic sublattices. Thus, following Lines and Jones, we obtain from Eq. (2')

$$\begin{aligned} \mathcal{H}_i = & -g\mu_B H_z S_{iz} \\ & - \sum_{j \neq i} [(J_{ij} - \frac{1}{2}J'_{ij}) \langle S_{iz} \rangle S_{iz} \\ & + J'_{ij} (\langle S_{iz}^2 \rangle S_{iz}^2 + \langle S_{jy}^2 \rangle S_{iy}^2 + \langle S_{jx}^2 \rangle S_{ix}^2)]. \end{aligned} \quad (3)$$

By virtue of the fact that $S_{ix}^2 + S_{iy}^2 + S_{iz}^2 = S_i^2$ and that

$$\langle S_{ix}^2 \rangle = \langle S_{jy}^2 \rangle = \frac{1}{2}[S(S+1) - \langle S_{iz}^2 \rangle],$$

Eq. (3) can be written as

$$\begin{aligned} \mathcal{H}_i = & -[g\mu_B H_z + (J_0 - \frac{1}{2}J'_0) \langle S_z \rangle] S_{iz} \\ & - \frac{1}{2}J'_0 [3 \langle S_z^2 \rangle - S(S+1)] S_{iz}^2 \\ & + \frac{1}{2}J'_0 [\langle S_z^2 \rangle - S(S+1)] S_i^2, \end{aligned} \quad (4)$$

where $J_0 \equiv \sum_{j \neq i} J_{ij}$, $J'_0 \equiv \sum_{j \neq i} J'_{ij}$, and the j in $\langle S_{jz} \rangle$ and $\langle S_{jz}^2 \rangle$ has been dropped because all the magnetic atoms are considered equivalent. If we use

the Stevens quadrupole operator, $O_2^0 = 3S_z^2 - S(S+1)$, the last two terms on the right in Eq. (4) become $-\frac{1}{6}J'_0 [\langle O_2^0 \rangle O_2^0 - 2S(S+1)S_i^2]$, thus showing the well-known equivalence between biquadratic and quadrupole coupling. These terms reduce to a constant for $S = \frac{1}{2}$; biquadratic interactions have no effect on the thermodynamic properties of a spin- $\frac{1}{2}$ system. Since \mathcal{H}_i in Eq. (4) is diagonal in S_{iz} , the eigenenergies are

$$\begin{aligned} E_m = & -[g\mu_B H_z + (J_0 - \frac{1}{2}J'_0) \langle S_z \rangle] m \\ & - \frac{1}{2}J'_0 [3 \langle S_z^2 \rangle - S(S+1)] m^2 \\ & + \frac{1}{2}J'_0 [\langle S_z^2 \rangle - S(S+1)], \end{aligned} \quad (5)$$

where m is an eigenvalue of S_{iz} . For consistency within the model, $\langle S_{iz} \rangle = \langle S_z \rangle$ and $\langle S_{iz}^2 \rangle = \langle S_z^2 \rangle$, and the expressions for these thermal averages are

$$\langle S_z \rangle = \sum_m m e^{-E_m/kT} / \sum_m e^{-E_m/kT} \quad (6a)$$

and

$$\langle S_z^2 \rangle = \sum_m m^2 e^{-E_m/kT} / \sum_m e^{-E_m/kT}, \quad (6b)$$

where the summations scan the m values: $-S, -S+1, \dots, S-1, S$.

Although, in principle, a self-consistent solution of Eqs. (5), (6a), and (6b) would give $\langle S_z \rangle$ as a function of H_z and T , the complexity of the problem under general conditions would require that the solution be numerical. To obtain an analytical solution, we resort to an expansion effectively in terms of J'_0/kT . The details of this procedure are described in Appendix A. We show that in the equation of state written as

$$\langle S_z \rangle / S = B_s(g\mu_B S H_{eff}/kT), \quad (7)$$

where B_s is the Brillouin function, the total effective field H_{eff} can be expressed as follows:

$$\begin{aligned} g\mu_B H_{eff} = & g\mu_B H_z + (J_0 - \frac{1}{2}J'_0) \langle S_z \rangle \\ & + \sum_n A_n (J'_0/kT)^n J'_0 \langle S_z \rangle^3 \\ & + \sum_n B_n (J'_0/kT)^n J'_0 \langle S_z \rangle^5 + \dots, \end{aligned} \quad (8)$$

where $n=0, 1, 2, \dots$. The coefficients A_n and B_n are numerical functions of S (which are zero for any n if $S = \frac{1}{2}$) and are given in Appendix A. Equation (8) can obviously be converted to an expression for the exchange field $H_{exch} (= H_{eff} - H_z)$, which for $|J'_0| \ll kT$ is simply

$$H_{exch} = (\lambda_0 - \frac{1}{2}\lambda'_0 g^2 \mu_B^2) M + A_0 \lambda'_0 M^3 + \dots, \quad (9)$$

where $\lambda_0 = J_0/g^2\mu_B^2$, $\lambda'_0 = J'_0/g^4\mu_B^4$, and $M = g\mu_B\langle S_z \rangle$, the average moment per magnetic atom.

Since λ'_0 represents the biquadratic part of the spin Hamiltonian, Eq. (9) shows that biquadratic interactions in a paramagnetic system (of $S \geq 1$) cause the net exchange field to contain cubic (and higher-order) terms in the induced magnetization. This result clearly provides a plausible explanation for the paramagnetic H_{exch} vs M characteristics of PrAg and $\text{Pr}_{0.5}\text{La}_{0.5}\text{Ag}$, as expressed in Eq. (1'). In relating λ' and $A_0\lambda'_0$, the coefficients of M^3 in Eqs. (1') and (9), we note in Table I that the λ' values for both compounds are negative, and since A_0 is positive, the corresponding values of λ'_0 are also negative. A negative λ'_0 , in turn, corresponds to a negative value for the j summation of J_{ij} in Eq. (2), which means that predominantly the biquadratic interactions favor quadrature rather than collinear spin alignment. Hence, in these materials, the biquadratic and bilinear interactions must be in competition since the latter always favor a collinear spin alignment.

In the theoretical problem of the antiferromagnetic properties of PrAg in an external field, which is discussed in Sec. III B, the mean-field Hamiltonian analogous to Eq. (4) would be much too complicated to allow analytical solution. However, by following a simplified mean-field approach, we manage to obtain analytical expressions that predict a physically reasonable behavior for each property of interest. In order that a valid analytical connection can later be made between the properties of PrAg above and below T_N , we will now follow the same simplified approach for the paramagnetic state. Hence, we set $\langle S_{j\alpha}S_{j\beta} \rangle = \langle S_{j\alpha} \rangle \langle S_{j\beta} \rangle$ in Eq. (2'), which for $H_x = H_y = 0$ becomes simply

$$\mathcal{H}_i = -(g\mu_B H_x + J_0 \langle S_z \rangle) S_{iz} - J'_0 \langle S_z \rangle^2 S_{iz}^2, \quad (10)$$

where J_0 and J'_0 are defined as before. Here \mathcal{H}_i is diagonal in S_{iz} and thus gives immediately

$$E_m = -(g\mu_B H_x + J_0 \langle S_z \rangle) m - J'_0 \langle S_z \rangle^2 m^2 \quad (11)$$

for the eigenenergies, where m is an eigenvalue of S_{iz} . For an analytical expression for H_{eff} , we again resorted to an expansion effectively in terms of J'_0/kT . As described in Appendix A, when H_{eff} is defined by Eq. (7), it again has the form given by Eq. (8), except that $\frac{1}{2}J'_0$ is omitted from the coefficient of $\langle S_z \rangle$. Thus, the exchange field can be written as

$$H_{\text{exch}} = \lambda_0 M + A'_0 \lambda'_0 M^3 + \dots, \quad (12)$$

where λ_0 and λ'_0 are defined as before, and A'_0 and higher-order coefficients are given in Appendix A.

dix A.

Clearly, even in this simplified mean-field approximation, the biquadratic interactions in a paramagnetic system generate cubic and higher-order terms in M in the expression for H_{exch} . Hence, similar to Eq. (9), Eq. (12) provides a simple theoretical rationale for the paramagnetic behavior of PrAg and $\text{Pr}_{0.5}\text{La}_{0.5}\text{Ag}$. Our qualitative comments about the negative values of λ'_0 for these materials are still valid. Quantitatively, we can identify Eq. (12) with Eq. (1'), such that $\lambda_0 = \lambda$ and $A'_0 \lambda'_0 = \lambda'$, and use the λ and λ' values in Table I for the two compounds considered as $S = 1$ systems. Thus, also using $A'_0 = \frac{1}{2}$ for $S = 1$, we obtain for PrAg at 10°K

$$\lambda_0 = 45.6 \text{ kOe}/\mu_B, \quad \lambda'_0 = -9.2 \text{ kOe}/\mu_B^3, \quad (13a)$$

and for $\text{Pr}_{0.5}\text{La}_{0.5}\text{Ag}$ at 4.2°K

$$\lambda_0 = 14.4 \text{ kOe}/\mu_B, \quad \lambda'_0 = -10.2 \text{ kOe}/\mu_B^3. \quad (13b)$$

It is obvious from these values that the net biquadratic coupling is roughly the same in the two compounds and, in the case of $\text{Pr}_{0.5}\text{La}_{0.5}\text{Ag}$, is comparable in strength to the net bilinear coupling. The values of these exchange parameters for PrAg will be discussed below with reference to our analysis of its antiferromagnetic behavior.

B. Antiferromagnetic state

With regard to its ordered antiferromagnetic state, we will continue to characterize PrAg by its crystal-field ground-state triplet and thus consider it effectively as a spin-1 system. Moreover, the Hamiltonian in Eq. (2') will be assumed to remain valid below the Néel temperature, except that the interaction summations over neighboring atoms will now involve the spins on two different sublattices. Our primary interest being the canted spin-flopped state (and its anomalous magnetization behavior described earlier), we set the sublattice moments along the $\pm z$ directions and allow them to deviate symmetrically from these directions in response to an external field in the x direction. Unfortunately, under these conditions, the solution of Eq. (2') for the eigenenergies is extremely difficult. To make this equation tractable, we set $\langle S_{j\alpha}S_{j\beta} \rangle = \langle S_{j\alpha} \rangle \langle S_{j\beta} \rangle$, thus neglecting spin correlations, and obtain the following expressions for the Hamiltonian of the i th spin on sublattice A (the other sublattice being B):

$$\mathcal{H}_i^A = -g\mu_B H_x S_{ix}^A - J_1 P_1 - J_2 P_2 - J'_1 P_1^2 - J'_2 P_2^2, \quad (14)$$

where

$$J_1 \equiv \sum_{j \neq i} J_{ij}, \quad J_2 \equiv \sum_j J_{ij}, \quad J'_1 \equiv \sum_{j \neq i} J'_{ij}, \quad J'_2 \equiv \sum_j J'_{ij},$$

$$P_1 \equiv \langle S_{ix}^A \rangle S_{ix}^A + \langle S_{ix}^B \rangle S_{ix}^B, \quad P_2 \equiv \langle S_{ix}^B \rangle S_{ix}^A + \langle S_{ix}^A \rangle S_{ix}^B.$$

An interchange of A and B produces an equivalent expression for \mathcal{H}_i^B . Furthermore, from symmetry we have $\langle S_{ix}^A \rangle = \langle S_{ix}^B \rangle \equiv \langle S_x \rangle$ and $\langle S_{ix}^A \rangle = -\langle S_{ix}^B \rangle \equiv \langle S_z \rangle$. Hence, Eq. (14) can be written without superscripts for either sublattice as follows:

$$\begin{aligned} \mathcal{H}_i = & -[g\mu_B H_x + (J_1 + J_2)\langle S_x \rangle]S_{ix} - (J_1 - J_2)\langle S_z \rangle S_{iz} \\ & - (J'_1 + J'_2)(\langle S_x \rangle^2 S_{ix}^2 + \langle S_z \rangle^2 S_{iz}^2) \\ & - (J'_1 - J'_2)\langle S_x \rangle \langle S_z \rangle (S_{ix} S_{iz} + S_{iz} S_{ix}), \end{aligned} \quad (15)$$

where subscripts 1 and 2 continue to refer to the interactions within and between sublattices, respectively.

Though Eq. (15) is valid for any S, our particular concern here is the case of $S=1$ ($g=2$), which pertains most closely to PrAg. Various aspects of this case, corresponding to various thermodynamic properties derived from the eigenvalues of the Hamiltonian (15), are discussed in detail in Appendix B. In particular, the dependence of the average magnetization $M(=g\mu_B \langle S_x \rangle)$ on the external field $H(=H_x)$ is found to obey the following relationship at $T=0$:

$$\begin{aligned} H = & -2(\lambda_2 - 4\lambda'_2 \mu_B^2)M \\ & - 4\lambda'_2 [1 + 4\lambda'_2 \mu_B^2 / (\lambda_1 - \lambda_2)] M^3 + \dots, \end{aligned} \quad (16)$$

where

$$\lambda_{1,2} \equiv J_{1,2} / (2\mu_B)^2, \quad \lambda'_{1,2} \equiv J'_{1,2} / (2\mu_B)^4.$$

This equation relates specifically to the spin-flopped state and, consequently, the reciprocal of the coefficient of M represents the perpendicular susceptibility at low fields, i.e.,

$$\chi_\perp = -1/2(\lambda_2 - 4\lambda'_2 \mu_B^2) \quad (17)$$

at $T=0$. Aside from zero-point energy effects, the corresponding parallel susceptibility (χ_\parallel) can be expected to be zero. In comparison, the initial susceptibility at the Néel point,

$$\chi(T_N) = -1/2\lambda_2, \quad (18a)$$

and the Néel temperature itself,

$$T_N = \frac{3}{2}(\lambda_1 - \lambda_2)\mu_B^2/k, \quad (18b)$$

as also shown in Appendix B.

Since $\chi(T_N)$ is positive, λ_2 has to be negative, which simply reflects the fact that the net bilinear coupling between sublattices is antiferromagnetic. If λ'_2 is also negative, it follows from Eqs. (17) and (18a) and the condition, $\chi_\parallel = 0$, that the powder susceptibility, $\frac{1}{2}(2\chi_\perp + \chi_\parallel)$, at $T=0$ may actually exceed the susceptibility at T_N . Thus, the peculiar low temperature increase that we have observed in the initial susceptibility of a polycrystalline sample of PrAg can be ascribed to a negative λ'_2 , corresponding to a net biquadratic coupling between sublattices that favors quadrature spin alignment. The role of λ'_2 in PrAg is made even clearer when the anomalous magnetization versus field behavior of the material in its spin-flopped state is interpreted in the light of Eq. (16). As shown in Fig. 2, the observed behavior at 4.2°K is represented above the critical field by the relation, $H = cM^3$, where $c = 18.5 \text{ kOe}/\mu_B^3$. Hence, a comparison with Eq. (16), though strictly valid only at $T=0$, gives

$$\lambda_2 - 4\lambda'_2 \mu_B^2 = 0, \quad (19a)$$

and

$$-4\lambda'_2 [1 + 4\lambda'_2 \mu_B^2 / (\lambda_1 - \lambda_2)] = 18.5 \text{ kOe}/\mu_B^3. \quad (19b)$$

Equation (19a) may be taken to signify that in PrAg at 4.2°K there is a balance between the negative biquadratic and negative bilinear interactions between sublattices, in their respective favoring of quadrature and antiparallel spin alignment. In fact, if $-4\lambda'_2 \mu_B^2$ were larger than $-\lambda_2$, such that the coefficient of M in Eq. (16) became negative, this equation would predict a spontaneous magnetization arising from a canting of the sublattice moments in zero external field. This zero-field canted state may actually exist in PrAg at very low temperature, as will be discussed below.

For a quantitative estimate of the exchange coefficients for PrAg, we start with the results given in Eq. (13a) for the paramagnetic state close to the Néel point. Since each of λ_3 and λ'_3 represents an algebraic sum of the interactions within and between sublattices, these results can be expressed as

$$\lambda_1 + \lambda_2 = 45.6 \text{ kOe}/\mu_B \quad (20a)$$

and

$$\lambda'_1 + \lambda'_2 = -9.2 \text{ kOe}/\mu_B^3. \quad (20b)$$

For the individual bilinear-exchange coefficients (λ_1, λ_2), we substitute our experimental values, $\chi(T_N) = 0.070 \mu_B/\text{kOe}$ and $T_N = 11^\circ\text{K}$, into Eqs. (18a) and (18b) and obtain from their combination

$$\lambda_1 = 54.3 \text{ kOe}/\mu_B, \quad \lambda_2 = -7.1 \text{ kOe}/\mu_B. \quad (21)$$

These results give $\lambda_1 + \lambda_2 = 47.2 \text{ kOe}/\mu_B$, in very good agreement with Eq. (20a). It follows from (21) that the positive value of $\lambda_1 + \lambda_2$, which corresponds in Fig. 4 to the downward displacement of the experimental χ_0^{-1} vs T curve from the calculated (dotted) curve for the noninteracting spin-1 system at T_N , reflects the fact that the net bilinear coupling in PrAg is ferromagnetic within the sublattices and relatively weakly antiferro-

magnetic between them.

In determining the biquadratic-exchange coefficients (λ'_1, λ'_2) individually, it might appear that Eq. (20b) can be used in conjunction with Eq. (19b) under the assumption that the latter equation continues to represent quantitatively the cubic part of the M vs H curve for PrAg down to 0°K. [Presumably, Eq. (19a) does not hold at 0°K since it would require a continued balance between the opposing effects of λ'_2 and λ'_2 .] However, for the λ_1 and λ_2 values given in (21), the left side of Eq. (19b) can only reach a maximum level of 15.4 kOe/ μ_B^3 , corresponding to $\lambda'_2 = -7.7$ kOe/ μ_B^3 . If a λ'_2 of even approximately this value were valid, the coefficient of M in Eq. (16) would be sizably negative, which would signify a nonzero spontaneous magnetization at 0°K, as was mentioned earlier. Unfortunately, our measurements do not extend below 4.2°K, and the possibility that PrAg has a zero-field canted state at lower temperatures can only be offered as a speculation (although a previous unpublished report¹⁵ does present experimental evidence for a zero-field magnetization at ~2°K). The only firm quantitative statement we can make at present about the biquadratic interactions in PrAg is given in Eq. (20b). Qualitatively, however, we have shown that these higher-order interactions are sufficiently strong for them to play a very important role in the magnetic properties of this material.

IV. DISCUSSION

Some of the earliest interest in biquadratic exchange coupling and its effect on magnetic properties was with regard to certain compounds of manganese.^{14,16,17} In fact, the paper by Lines and Jones,¹⁴ whose approach was followed in writing the mean-field Hamiltonian of Eq. (3), was concerned specifically with α -MnS. From an analysis of NMR data for the sublattice magnetization versus temperature, they concluded that nearest-neighbor biquadratic interactions in this antiferromagnetic compound play a fairly insignificant role. This is essentially what they concluded earlier regarding MnO.¹⁷

More recently, most experimental and theoretical investigations concerned with biquadratic interactions have involved various compounds of the rare earths. Particularly in the case of ionic insulators, there are many examples in which these higher-order interactions have been shown to be comparable in strength to the normal bilinear coupling.¹⁸ However, in the case of rare-earth intermetallic compounds, which pertains more directly to our study of PrAg, experimental evidence for the existence of biquadratic exchange

has only been reported for a small number of materials. Among these, only the pseudobinary (Tb,Y)Sb compounds, which are singlet ground-state systems, have been studied magnetically in any manner analogous to that of the present work on PrAg. It appears, however, that although the measured M vs H isotherms for the paramagnetic (Tb,Y)Sb compounds¹⁹ are consistent with a higher-order dependence of the exchange field on M , similar to that of Eq. (1'), the temperature dependence of the sublattice magnetization of the antiferromagnetic compounds²⁰ gives no supportive evidence that the exchange field varies other than linearly with M .

To date, the most conclusive indication of biquadratic coupling in rare-earth intermetallic compounds has emerged from the results of ultrasonic vibrational measurements on DySb,^{21,22} and HoSb.²² The pronounced elastic-constant softening observed in these materials just above their magnetic (and structural transition) temperatures was attributed in large part to magnetic quadrupole-quadrupole (effectively biquadratic) interactions, where the quadrupoles are coupled to the lattice strains. Presumably, the same type of interactions are responsible for the elastic-constant softening seen in TmCd as this CsCl-structured compound, which does not order magnetically, approaches its structural transition temperature from above.²³ Furthermore, in the case of DySb, the first-order transition to an antiferromagnetic state has been shown to be consistent with a net biquadratic coupling that is positive and thus favors collinear arrangement of the spins.²⁴ It should be noted, however, that DySb also undergoes a field-induced transition to a state where the sublattice moments are in quadrature,²⁵ which suggests that at high fields the effective biquadratic coupling may be negative (which, as we have shown, is the situation in PrAg at all fields). Pertinent to this question, an extensive phenomenological study has been made of the different types of ordered states that can occur at various temperatures in a spin-1 system due to the coexistence of bilinear and biquadratic coupling of either sign.²⁶ Since this study was restricted to collinear magnetic ordering, it does not encompass the possibility of a canted spin state, whereas such a state is expressly allowed (even at zero field) by our simplified Hamiltonian analysis of the magnetic properties of PrAg below its Néel point.

In theoretical discussions of DySb,^{21,22,24,27} the biquadratic interactions have generally been ascribed to either or both of two sources. One is the mechanism whereby the magnetic quadrupoles of the rare-earth atoms are coupled via the co-

herent dynamical distortions of the local crystal fields, produced by the phonons in the system. This "virtual phonon exchange" process, which has recently been reviewed in detail,²⁸ can give rise to an effective biquadratic coupling of considerable range. The other biquadratic coupling mechanism, which also is inherently long range and is specifically relevant to intermetallics, is a higher-order component of the indirect exchange interactions via the conduction electrons. Higher-order indirect exchange coupling has recently been calculated to be of significant strength in DyZn,²⁹ which resembles PrAg in its CsCl-type structure. Although it has been impossible to distinguish between these two mechanisms experimentally on the basis of available data, we are planning to accomplish this for PrAg by means of detailed neutron scattering measurements of the magnon and phonon spectra.

ACKNOWLEDGMENTS

We are grateful to P. M. Levy, M. Blume, B. R. Cooper, L. F. Uffer, and S. T. Chiu-Tsao for enlightening discussions about biquadratic exchange, and to G. P. Felcher for helpful discussions of our neutron-diffraction results. We also thank R. Aitken for his help in the magnetization measurements and J. F. Reddy for the sample preparation. One of us (J. S. K.) gratefully acknowledges the hospitality of the Solid State Science Division of the ANL during his recent sabbatical leave from the University of Illinois at Chicago Circle.

APPENDIX A

Following the notation of Lines and Jones,¹⁴ we define

$$X \equiv g\mu_B H_z + (J_0 - \frac{1}{2}J'_0) \langle S_z \rangle \quad (\text{A1a})$$

and

$$Y \equiv \frac{1}{2}J'_0 [3 \langle S_z^2 \rangle - S(S+1)], \quad (\text{A1b})$$

so that Eq. (5) can be written simply as

$$E_m = -Xm - Ym^2 + E_0, \quad (\text{A2})$$

where $E_0 = \frac{1}{2}J'_0 [\langle S_z^2 \rangle - S(S+1)]$. Substituting (A2) into Eqs. (6a) and (6b) and factoring out E_0 , we obtain

$$\langle S_z \rangle = \sum_m m \exp[\beta(Xm + Ym^2)] / \sum_m \exp[\beta(Xm + Ym^2)] \quad (\text{A3a})$$

and

$$\langle S_z^2 \rangle = \sum_m m^2 \exp[\beta(Xm + Ym^2)] / \sum_m \exp[\beta(Xm + Ym^2)], \quad (\text{A3b})$$

where $\beta = 1/kT$ and $m = -S, -S+1, \dots, S-1, S$. Under the condition that $\beta(Xm + Ym^2) \ll 1$ for any m , the exponential is expanded as

$$\exp[\beta(Xm + Ym^2)] = \sum_{k=0, \dots} \zeta_k m^k,$$

where $\zeta_0 = 1$, $\zeta_1 = \beta X$, $\zeta_2 = \beta Y + \frac{1}{2}\beta^2 X^2$, etc., and Eqs. (A3a) and (A3b) become

$$\langle S_z \rangle = \sum_k \alpha_{k+1} \zeta_k / \sum_k \alpha_k \zeta_k \quad (\text{A4a})$$

and

$$\langle S_z^2 \rangle = \sum_k \alpha_{k+2} \zeta_k / \sum_k \alpha_k \zeta_k, \quad (\text{A4b})$$

where $\alpha_k = \sum_m m^k$, which is nonzero only for k even.

From (A4b) and (A1b), we obtain Y as a series expansion in even (but nonzero) powers of X , which we then substitute into (A4a) and obtain $\langle S_z \rangle$ as a series expansion in odd powers of X . The latter series is inverted to give

$$X = \gamma_1 \langle S_z \rangle + (\gamma_3 - \rho_3) \langle S_z \rangle^3 + (\gamma_5 - \rho_5) \langle S_z \rangle^5 + \dots, \quad (\text{A5})$$

which is so written that the γ 's depend only on β and S and the ρ 's are functions of J'_0 as well as β and S . Moreover, we obtain

$$\gamma_1 \langle S_z \rangle + \gamma_3 \langle S_z \rangle^3 + \gamma_5 \langle S_z \rangle^5 + \dots = (\beta S)^{-1} B_4^{-1}(\langle S_z \rangle / S),$$

where B_4^{-1} is the inverse Brillouin function. Hence, (A5) may be expressed as

$$\beta S [X + \rho_3 \langle S_z \rangle^3 + \rho_5 \langle S_z \rangle^5 + \dots] = B_4^{-1}(\langle S_z \rangle / S). \quad (\text{A6})$$

From this form of the equation of state, it is clear that the terms between the brackets constitute $g\mu_B H_{\text{eff}}$, where H_{eff} is the total effective field on each paramagnetic atom. Thus, from the definition of X in (A1a),

$$g\mu_B H_{\text{eff}} = g\mu_B H_z + (J_0 - \frac{1}{2}J'_0) \langle S_z \rangle + \rho_3 \langle S_z \rangle^3 + \rho_5 \langle S_z \rangle^5 + \dots, \quad (\text{A7})$$

where it is found that

$$\rho_3 = \sum_n A_n (\beta J'_0)^n J'_0, \quad \rho_5 = \sum_n B_n (\beta J'_0)^n J'_0, \dots;$$

$$A_0 = \frac{1}{16} b_{3/4}^2, \quad A_n = \frac{1}{12} b_{3/4} A_{n-1} \quad \text{for } n \geq 1;$$

$$B_0 = \frac{27}{128} b_{3/4}^2 b_{-3/16} / S(S+1), \quad B_1 = \frac{9}{256} b_{3/4}^2 b_{-3/2} S(S+1),$$

$$b_q \equiv [1 - q/S(S+1)] / (1 - \frac{1}{2}q).$$

Note that $b_{3/4}$, which is contained in A_n and B_n for all n , is zero for $S = \frac{1}{2}$. Hence, in (A7) the cubic and higher-odd-order terms in $\langle S_z \rangle$ are nonzero only if $S \geq 1$.

In the simplified mean-field approximation for

which the eigenenergies for the paramagnetic state are given in Eq. (11), we need only be concerned with $\langle S_z \rangle$ as expressed in (A3a), but where now

$$X = g\mu_B H_z + J_0 \langle S_z \rangle, \quad Y = J'_0 \langle S_z \rangle^2. \quad (\text{A8})$$

Again, for $\beta(Xm + Ym^2) \ll 1$, Eq. (A3a) can be written as (A4a), from which by virtue of (A8) we proceed directly to (A5). The latter equation is again expressible as (A6), from which we now obtain

$$g\mu_B H_{\text{eff}} = g\mu_B H_z + J_0 \langle S_z \rangle + \rho_3 \langle S_z \rangle^3 + \dots, \quad (\text{A9})$$

where the ρ 's have the same form as in (A7), but with different numerical coefficients, i.e.,

$$\rho_3 = \sum_n A'_n (\beta J'_0)^n J'_0, \quad \rho_5 = \sum_n B'_n (\beta J'_0)^n J'_0, \dots;$$

$$E_n^3 + 2C[\langle S_x \rangle^2 + \langle S_z \rangle^2] E_n^2 - [A^2 \langle S_x \rangle^2 + B^2 \langle S_z \rangle^2 - C^2(\langle S_x \rangle^2 + \langle S_z \rangle^2) - (C^2 - D^2)\langle S_x \rangle^2 \langle S_z \rangle^2] E_n$$

$$- [(A^2 + B^2)C - 2AED - (C^2 - D^2)C(\langle S_x \rangle^2 + \langle S_z \rangle^2)] \langle S_x \rangle^2 \langle S_z \rangle^2 = 0, \quad (\text{B1})$$

where

$$A = J_1 + J_2 + 2\mu_B H_z / \langle S_x \rangle, \quad B = J_1 - J_2,$$

$$C = J'_1 + J'_2, \quad D = J'_1 - J'_2.$$

In principle, with the solutions for E_n , the magnetization can be obtained from its statistical-mechanical definition,

$$M_x = 2\mu_B \langle S_x \rangle = - \sum_n \left(\frac{\partial E_n}{\partial H_x} \right)_{\mu_x} e^{-\beta E_n} / \sum_n e^{-\beta E_n}. \quad (\text{B2})$$

However, the general solution for $M_x(H_x, T)$ is a very complicated analytical problem and will not be pursued further here.

It serves our present purposes to consider the situation at $T=0$, for which (B2) reduces to

$$M_x = - \left(\frac{\partial E_1}{\partial H_x} \right)_{\mu_x}, \quad (\text{B3})$$

where E_1 is the ground-state energy. Furthermore, at $T=0$, we also have the simplifying relationship

$$\langle S_x \rangle^2 + \langle S_z \rangle^2 = 1,$$

which we use to eliminate $\langle S_z \rangle$ from (B1). Following this tactic, we solve (B1) and obtain E_1 as a power series in $\langle S_x \rangle^2$, namely,

$$E_1 = E_{10} + E_{12} \langle S_x \rangle^2 + E_{14} \langle S_x \rangle^4 + \dots, \quad (\text{B4})$$

where $E_{10} = -B - C$ and E_{12}, E_{14}, \dots are complicated functions of A, B, C , and D . Substitution of (B4) into (B3) gives

$$A'_0 = \frac{1}{2} b_{3/4}, \quad A'_n = 0 \quad \text{for } n \neq 1;$$

$$B'_0 = \frac{1}{8} b_{3/4} b_{-3/16} / S(S+1), \quad B'_1 = -\frac{1}{8} b_{3/4} b_{-11/12} S(S+1),$$

$$B'_n = 0 \quad \text{for } n \geq 2,$$

where b_n is defined as before. Since $b_{3/4} = 0$ for $S = \frac{1}{2}$, we again have that in the expression for H_{eff} the cubic and higher-odd-order terms in $\langle S_z \rangle$ are nonvanishing only if $S \geq 1$.

APPENDIX B

Although the Hamiltonian in Eq. (15) for the ordered magnetic state is nondiagonal, we are fortunately interested in the relatively simple case of $S=1$. In this case, the cubic secular equation for the eigenenergies is as follows:

$$M_x = - \frac{\partial E_{12}}{\partial H_x} \langle S_x \rangle^2 - \frac{\partial E_{14}}{\partial H_x} \langle S_x \rangle^4 - \dots,$$

since $\partial E_{10} / \partial H_x = 0$. From the definitions of A and M_x , the latter equation can be written as

$$- \frac{\partial E_{12}}{\partial A} - \frac{\partial E_{14}}{\partial A} \langle S_x \rangle^2 - \dots = 1,$$

from which we find

$$A = B + C - D - 2(C - D)[1 + (C - D)/2B] \langle S_x \rangle^2 + \dots.$$

Thus, from the definitions of A, B, C , and D ,

$$\mu_B H_x = - (J_2 - J'_2) \langle S_x \rangle - 2J'_2 [1 + J'_2 / (J_1 - J_2)] \langle S_x \rangle^3 + \dots,$$

which leads directly to Eq. (16) for M_x vs H_x at $T=0$.

In the absence of H_x , $\langle S_x \rangle = 0$ and (B1) reduces to

$$E_n^3 + 2C \langle S_z \rangle^2 E_n^2 - [B^2 \langle S_z \rangle^2 - C^2 \langle S_z \rangle^4] E_n = 0,$$

whose solutions are

$$E_n = 0, \pm B \langle S_z \rangle - C \langle S_z \rangle^2. \quad (\text{B5})$$

Furthermore, since the Hamiltonian (15) is now diagonal in $\langle S_z \rangle$, it follows from Eqs. (B5) and (6a) that

$$\langle S_z \rangle = \frac{e^{\beta B \langle S_z \rangle} - e^{-\beta B \langle S_z \rangle}}{e^{\beta B \langle S_z \rangle} + e^{-\beta B \langle S_z \rangle} + e^{-\beta C \langle S_z \rangle^2}} \quad (\text{B6})$$

which gives the sublattice magnetization ($2\mu_B \langle S_z \rangle$)

as a function of temperature up to the Néel point (T_N). To obtain T_N , we let $\langle S_x \rangle$ in (B6) become vanishingly small and find that

$$T_N = 2B/3k = 2(J_1 - J_2)/3k. \quad (B7)$$

For the susceptibility at T_N , we let $\langle S_x \rangle = 0$ in (B1), which now reduces to

$$E_n^2 + 2C\langle S_x \rangle^2 E_n - (A^2\langle S_x \rangle^2 - C^2\langle S_x \rangle^4)E_n = 0.$$

Hence, the eigenenergies are

$$E_n = 0, \pm A\langle S_x \rangle - C\langle S_x \rangle^2,$$

which, substituted into (B2), yield

$$\langle S_x \rangle = \frac{e^{\beta_N A \langle S_x \rangle} - e^{-\beta_N A \langle S_x \rangle}}{e^{\beta_N A \langle S_x \rangle} + e^{-\beta_N A \langle S_x \rangle} + e^{-\beta_N C \langle S_x \rangle^2}}, \quad (B8)$$

where $\beta_N = 1/kT_N$. Through the dependence of A on H_x , (B8) describes the induced magnetization ($2\mu_B \langle S_x \rangle$) at T_N as a function of H_x . For very small values of H_x and $\langle S_x \rangle$, (B8) reduces to

$$\langle S_x \rangle = \beta_N A \langle S_x \rangle = 2[(J_1 + J_2)\langle S_x \rangle + 2\mu_B H_x]/3kT_N$$

which, combined with (B7), gives

$$\chi = 2\mu_B \langle S_x \rangle / H_x = -2\mu_B^2 / J_2$$

for the initial susceptibility at T_N .

†Work performed under the auspices of the U. S. Energy Research and Development Administration.

*Permanent address: Department of Physics, University of Illinois, Chicago, Ill. 60680. Work supported in part by the National Science Foundation and the Office of Naval Research.

¹T. O. Brun, G. H. Lander, D. L. Price, G. P. Felcher, and J. F. Reddy, Phys. Rev. B **9**, 248 (1974).

²K. H. Buschow, J. P. de Jong, H. W. Zandbergen, and B. van Laar, J. Appl. Phys. **46**, 1352 (1975).

³J. W. Cable, W. C. Koehler, and E. O. Wollan, Phys. Rev. **136**, A240 (1964).

⁴G. Arnold, N. Nereson, and C. Olsen, J. Chem. Phys. **46**, 4041 (1967).

⁵N. Nereson, AIP Conf. Proc. **10**, 669 (1973).

⁶N. Nereson, J. Appl. Phys. **44**, 4727 (1973).

⁷R. E. Walline and W. E. Wallace, J. Chem. Phys. **41**, 3285 (1964).

⁸J. Pierre and R. Pauthenet, C. R. Acad. Sci. (Paris) **260**, 2739 (1965).

⁹T. O. Brun, J. S. Kouvel, G. H. Lander, and R. Aitken, Solid State Commun. **15**, 1157 (1974).

¹⁰Two alternative but similar crystal-field level schemes are proposed in Ref. 1 on the basis of neutron scattering data on PrAg. The scheme used in the present paper, corresponding to the parameters $W = -0.43$ meV and $\tau = -0.8$ is one of these alternatives and is favored by the results of recent unpublished neutron work on $\text{Pr}_{0.5}\text{La}_{0.5}\text{Ag}$ by the same researchers.

¹¹K. R. Lea, M. J. Leask, and W. P. Wolf, J. Phys. Chem. Solids **23**, 1381 (1962).

¹²R. J. Birgeneau, E. Bucher, L. Passell, D. L. Price, and K. C. Turberfield, J. Appl. Phys. **41**, 900 (1970).

¹³K. C. Turberfield, L. Passell, R. J. Birgeneau, and E. Bucher, Phys. Rev. Lett. **25**, 752 (1970); J. Appl. Phys. **42**, 1746 (1971).

¹⁴M. E. Lines and E. D. Jones, Phys. Rev. **141**, 525

(1966).

¹⁵J. Pierre, Ph.D. thesis (University of Grenoble, 1969) (unpublished).

¹⁶D. S. Rodbell, I. S. Jacobs, J. Owen, and E. A. Harris, Phys. Rev. Lett. **11**, 10 (1963); D. S. Rodbell and J. Owen, J. Appl. Phys. **35**, 1002 (1964).

¹⁷M. E. Lines, Phys. Rev. **139**, A1304 (1965); M. E. Lines and E. D. Jones, *ibid.* **139**, A1313 (1965).

¹⁸W. P. Wolf, J. Phys. (Paris) **32**, C1-26 (1971); J. M. Baker, Rep. Prog. Phys. **34**, 109 (1971).

¹⁹B. R. Cooper, I. S. Jacobs, C. D. Graham, and O. Vogt, J. Phys. (Paris) **32**, C1-359 (1971).

²⁰J. W. Cable, J. B. Comly, B. R. Cooper, I. S. Jacobs, W. C. Koehler, and O. Vogt, AIP Conf. Proc. **10**, 1554 (1973).

²¹T. J. Moran, R. L. Thomas, P. M. Levy, and H. H. Chen, Phys. Rev. B **7**, 3238 (1973).

²²M. E. Mullen, B. Lüthi, P. S. Wang, E. Bucher, L. D. Longinotti, J. P. Maita, and H. R. Ott, Phys. Rev. B **10**, 186 (1974).

²³B. Lüthi, M. E. Mullen, K. Andres, E. Bucher, and J. P. Maita, Phys. Rev. B **8**, 2639 (1973).

²⁴L. F. Uffer, P. M. Levy, and H. H. Chen, AIP Conf. Proc. **10**, 553 (1973).

²⁵P. Streiff, G. E. Everett, and A. W. Lawson, Phys. Lett. **50A**, 199 (1974); T. O. Brun, G. H. Lander, F. W. Korty, and J. S. Kouvel, AIP Conf. Proc. **21**, 244 (1975).

²⁶H. H. Chen and P. M. Levy, Phys. Rev. B **7**, 4267 (1973).

²⁷M. J. Sablik, H. H. Teitelbaum, and P. M. Levy, AIP Conf. Proc. **10**, 548 (1973); D. K. Ray and A. P. Young, J. Phys. C **6**, 3353 (1973).

²⁸G. A. Gehring and K. A. Gehring, Rep. Prog. Phys. **38**, 1 (1975).

²⁹D. K. Ray, Solid State Commun. **15**, 1471 (1974).

Appendix F

FIELD-INDUCED TRANSITIONS IN DySb*

T.O. Brun, G.H. Lander, F.W. Korty[†] and J.S. Kouvel[†]
Argonne National Laboratory, Argonne, Illinois 60439 and
University of Illinois, Chicago, Illinois 60680

ABSTRACT

The NaCl-structured compound DySb, which in zero field transforms abruptly at $T_N \approx 9.5$ K to a Type-II antiferromagnetic (A) state with a nearly tetragonal lattice distortion, was previously found to exhibit rapid field-induced changes in magnetization at 1.5 K. The field-induced transitions in a DySb crystal have been studied by neutron diffraction and magnetization measurements in fields up to ~ 60 kOe applied parallel to each of the principal axes. In the $\langle 100 \rangle$ case, the transition from the A to an intermediate ferrimagnetic (Q) state is first-order at 4.2 K (critical field $H_{c1} \approx 21$ kOe) but is continuous from ~ 6 K up to T_N , as $H_{c1} \rightarrow 0$. The Q-to-paramagnetic (P) transition is rapid but continuous at 4.2 K ($H_{c2} \approx 40$ kOe) and becomes broad as T_N is approached. In the $\langle 110 \rangle$ case the A-to-Q transition remains essentially first-order from 4.2 K ($H_{c1} \approx 15$ kOe) up to T_N ; above T_N rapid P-to-Q transitions occur at very high fields. The magnetic structure of the Q state is found to be that of HoP.

INTRODUCTION

In zero magnetic field, the compound DySb exhibits a first order magnetic transition^{1,2} at $T_N \approx 9.5$ K. Above T_N DySb has the cubic NaCl-structure. Below T_N the compound orders antiferromagnetically in the type-II structure that consists of ferromagnetic (111) planes stacked antiferromagnetically along the [111] axis. The first order transition is accompanied by a predominantly tetragonal lattice distortion ($c/a = .993$). The ordered magnetic moment at 6 K is $9.5 \mu_B$ per Dy, almost the saturation moment of $10 \mu_B$ for Dy^{3+} , and is parallel to the tetragonal [001] axis. Elastic as well as magneto-thermal data for DySb have been analyzed in a molecular field approximation,^{3,4} and the analysis shows that biquadratic pair interactions between the Dy^{3+} ions may be as important as the bilinear exchange.

Previous magnetization measurements⁵ made on a single crystal of DySb at 1.5 K in fields up to 60 kOe show that a ferrimagnetic state exists. For all three principal directions of the field the values of the magnetization in this state are consistent with the magnetic structure of DySb being that of HoP,⁶ in which the moments within each (111) plane of Dy atoms are ferromagnetically aligned with $10 \mu_B$ per Dy and oscillate between two perpendicular $\langle 100 \rangle$ directions in alternating (111) planes.

RESULTS

Magnetization measurements were performed on single crystals of DySb using a vibrating-sample magnetometer. Magnetic fields of up to 56 kOe were applied parallel to the $\langle 100 \rangle$, $\langle 110 \rangle$ and $\langle 111 \rangle$ crystallographic directions. The fields have been corrected for demagnetization. The results for the $\langle 100 \rangle$ direction are shown in Fig. 1 as isotherms M vs H . Below T_N we observe two critical fields at which the magnetization increases very rapidly. At 4.2 K the magnetization changes discontinuously at $H_{c1} \langle 100 \rangle = 21.6$ kOe and very rapidly at $H_{c2} \langle 100 \rangle = 40.6$ kOe. Both critical fields decrease with increasing temperature, both transitions becoming broader as the temperature approaches T_N . At 4.2 K the magnetization is almost $5 \mu_B$ per Dy atom just above $H_{c1} \langle 100 \rangle$ and approaches $10 \mu_B$ per Dy atom above $H_{c2} \langle 100 \rangle$.

In Fig. 2 the M vs H isotherms are shown for the field along $\langle 110 \rangle$. The isotherms show one transition which remains abrupt while its critical field, $H_{c1} \langle 110 \rangle$, decreases from 15.6 kOe at 4.2 K to zero at T_N . The magnetization at 4.2 K approaches a value of approximately $7.2 \mu_B$ at high fields. In addition, the

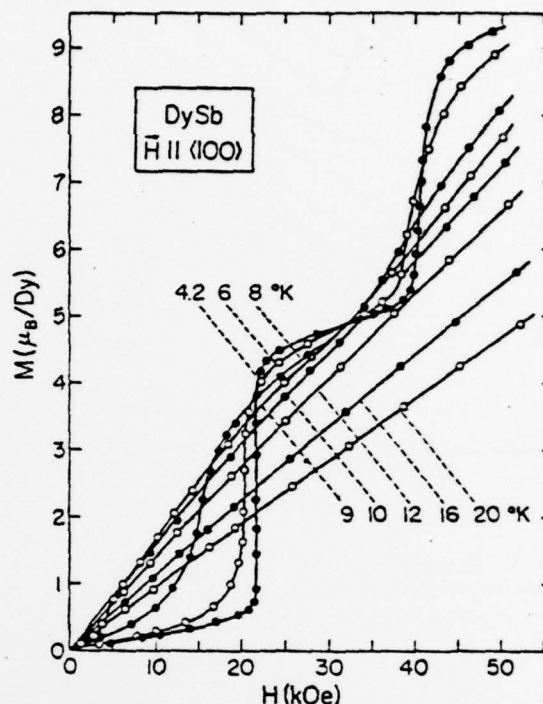


Figure 1. Magnetization of DySb vs. field applied along $\langle 100 \rangle$ at constant temperature.

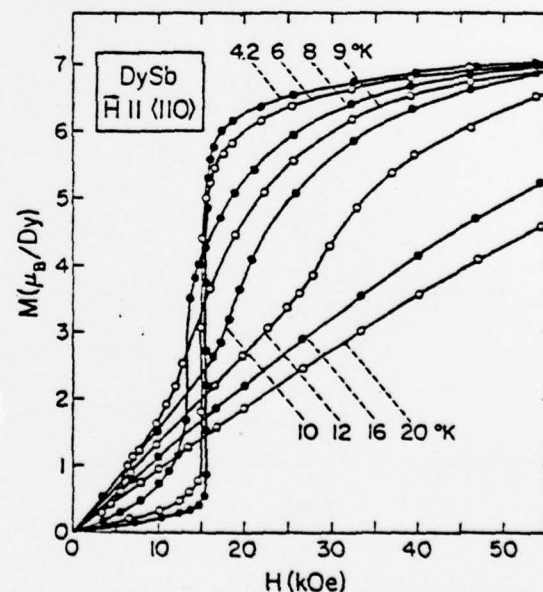


Figure 2. Same as Fig. 1 for field along $\langle 110 \rangle$.

isotherm for 9 K shows a very rapid increase in dM/dH at fields just above $H_{c1} \langle 110 \rangle$. The 10 K and 12 K isotherms above T_N show a similar change in dM/dH at fields just above 15 kOe and 26 kOe, respectively.

To determine the ranges of temperature and field for the various magnetic states of DySb, we have converted our data to field vs temperature curves of constant magnetization. The phase boundaries have been identified from the rapid changes in dH/dT . Fig. 3 shows the magnetic phase diagram for H parallel to

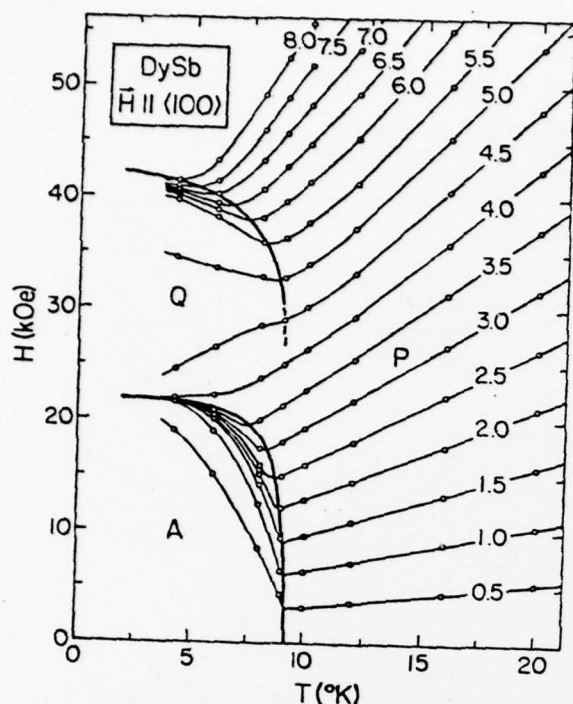


Figure 3. Field along $\langle 100 \rangle$ vs. temperature at constant magnetization (in μ_B/Dy) for DySb.

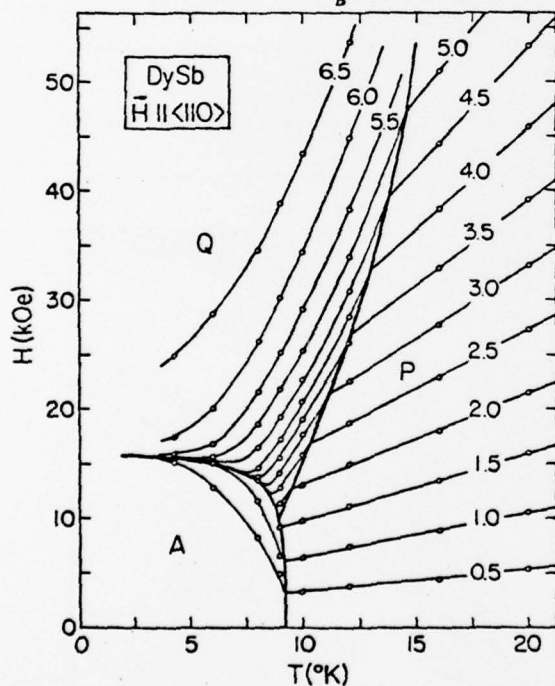


Figure 4. Same as Fig. 3 for field along $\langle 110 \rangle$. The phase marked P is paramagnetic, the A phase is the Type-II antiferromagnetic state, and the Q-phase is the intermediate ferrimagnetic state.

The magnetic phase diagram for H parallel to $\langle 110 \rangle$ is shown in Fig. 4. The P, A, and Q phases are the same as for H parallel to $\langle 100 \rangle$. An unusual feature of this diagram is that the boundary between the Q and P phases extends up to 15 K at the maximum field.

The magnetization data for $H \parallel \langle 111 \rangle$ are not shown, but the magnetic phase diagram is similar to that for

$H \parallel \langle 110 \rangle$. The critical field, $H_{c1} \langle 111 \rangle$, is 19 kOe at 4.2 K, and the value of the magnetization in the Q phase is $\sim 5.8 \mu_B$ per Dy atom.

Neutron diffraction measurements have been performed on a single crystal of DySb with $H \parallel [110]$ to determine the structure of the Q-phase. We have measured the integrated intensities of the $(\frac{1}{2} \frac{1}{2} \frac{1}{2})$ and the $(\frac{5}{2} \frac{3}{2} \frac{1}{2})$ antiferromagnetic reflections at 4.2 K and 11 K and for $H = 0$ and 30 kOe. The observed intensities for the Q-phase are in good agreement with $10 \mu_B$ per Dy parallel to $[100]$ and $[010]$ in alternate (111) planes. At 11 K no magnetic reflections are present in zero field, but by increasing the field the $(\frac{1}{2} \frac{1}{2} \frac{1}{2})$ -reflection appears at the P to Q boundary, with the same intensity as at 4.2 K. Preliminary data for the lattice distortions in the Q phase indicate that the lattice expands in the $[001]$ direction, normal to the plane of the moments.

DISCUSSION

The results of the present magnetization measurements are in good agreement with the results of Busch and Vogt.⁵ As pointed out by these authors the value of the magnetization in the Q phase for each of the three principal field directions is consistent with the HoP structure. Furthermore if the three Q phases have identical magnetic structures with the same exchange and anisotropy energies, the differences between the Zeeman energies of the three Q-phases predict that $H_{c1} \langle 100 \rangle = \sqrt{2} H_{c1} \langle 110 \rangle = 2/\sqrt{3} H_{c1} \langle 111 \rangle$. The experimental values of the three critical fields are in good agreement with this prediction. Both magnetization and neutron diffraction results for the Q-phase of DySb show therefore that this phase has the HoP structure with $10 \mu_B$ per Dy atom.

For $H \parallel \langle 100 \rangle$ the HoP structure cannot be stabilized by bilinear exchange interactions alone; additional couplings such as biquadratic pair interactions are needed. Stevens and Pytte⁷ have suggested that the dominant contribution to this biquadratic interaction comes from the couplings between the ion and the lattice. In their model cooperative shifts of the Sb ions relative to the Dy ions create local distortions stabilizing the HoP structure.

Further neutron diffraction measurements are required to verify the HoP structure of the Q phases for other direction of the field and to test the model of Stevens and Pytte.⁷ Our magnetization data for DySb above T_N are being compared in detail with crystal-field calculations of magnetization vs effective field in order to expose any evidence for biquadratic or any other higher-order coupling, as was done in a recent investigation of PrAg.⁸

*Based on work performed under the auspices of the U. S. Atomic Energy Commission.

†Supported in part by the Office of Naval Research.

REFERENCES

1. E. Bucher, R. J. Birgenau, J. P. Maita, G. P. Felcher and T. O. Brun, Phys. Rev. Letters **28**, 746 (1972).
2. G. P. Felcher, T. O. Brun, R. J. Gambino and M. Kuznietz, Phys. Rev. B **8**, 260 (1973).
3. T. J. Moran, R. L. Thomas, P. M. Levy and H. H. Chen, Phys. Rev. B **7**, 3238 (1973).
4. L. F. Uffer, P. M. Levy and H. H. Chen, AIP Conf. Proc. **10**, 553 (1973).
5. G. Busch and O. Vogt, J. Appl. Phys. **39**, 1334 (1968).
6. H. R. Child, M. K. Wilkinson, J. W. Cable, W. C. Koehler and E. O. Wollan, Phys. Rev. **131**, 922 (1963).
7. K. W. H. Stevens and E. Pytte, Solid State Comm. **13**, 101 (1973).
8. T. O. Brun, J. S. Kouvel, G. H. Lander and R. Aitken, Solid State Comm. **15**, 1157 (1974).

Appendix G

BIQUADRATIC EXCHANGE INTERACTIONS IN DySb*

J.S. KOUVEL,† T.O. BRUN and F.W. KORTY†

Argonne National Laboratory, Argonne, Illinois 60439, USA and University of Illinois, Chicago, Illinois 60680, USA

From a comparison of magnetization data on a DySb crystal above its Néel point with magnetization calculations based on its crystal-field states, it is shown that the exchange interactions have a substantial biquadratic component, as suggested by the field-induced state with orthogonal sublattice moments.

At the Néel temperature ($T_N \approx 9.5$ K) in zero magnetic field, the cubic NaCl-structured compound DySb transforms abruptly into a type-II antiferromagnet in which the Dy moments in adjacent ferromagnetic (111) planes are antiparallel [1, 2]. The first-order transition is accompanied by a nearly tetragonal lattice distortion and the ordered moments ($\sim 10 \mu_B/\text{Dy-atom}$) lie along the tetragonal [001] axis. Moreover, magnetic measurements [3] on a DySb crystal at 1.5 K have shown that the compound undergoes a rapid field-induced transition from the antiferromagnetic state to a state whose magnetization corresponds to an alignment of Dy moments in equal numbers along each of two orthogonal (100) directions. It was suggested [3] that the magnetic structure of this quadrature-spin (Q) state of DySb was that of HoP, in which the moments in adjacent ferromagnetic (111) planes are aligned orthogonally, and this has been borne out by neutron diffraction measurements on a DySb crystal in high fields [4]. The latter work [4] also included a magnetization study which gave a determination of the magnetic phase diagrams for the applied field (H) along (100) and (110). These are shown in fig. 1, together with the phase diagram for H along (111), which we recently determined from a similar study of the same DySb crystal. The nature and positions of the phase boundaries, plus the occurrence of tricritical points [5], will be discussed in a separate report.

For our present purpose, the magnetic phase diagrams for DySb serve to emphasize the high-field existence of the Q state, which cannot be stabilized by bilinear exchange interactions alone but requires higher-order interactions in

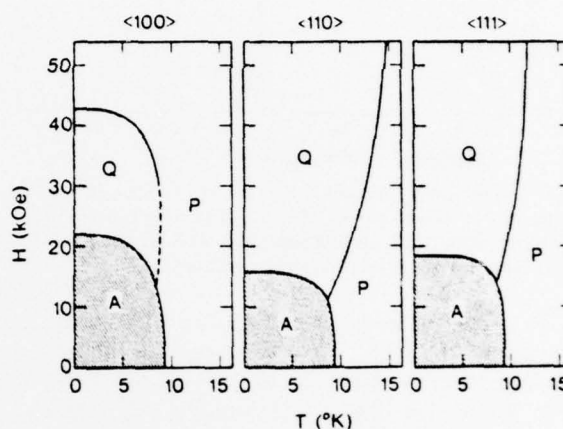


Fig. 1. Magnetic phase diagrams of field vs. temperature for DySb, indicating the antiferromagnetic (A), quadrature-spin (Q), and paramagnetic (P) regimes.

addition, as was pointed out earlier [4]. Specifically, if the higher-order interactions have a simple biquadratic form, the exchange hamiltonian (of the i th spin) can be written as

$$\mathcal{H}_i = - \sum_j [J_{ij} \mathbf{S}_i \cdot \mathbf{S}_j + J'_{ij} (\mathbf{S}_i \cdot \mathbf{S}_j)^2]. \quad (1)$$

The existence of the Q state would then suggest that the inter-sublattice component of the biquadratic exchange coefficient J'_{ij} is negative, thus favoring quadrature (orthogonal) over collinear alignment of the sublattice moments. The importance of biquadratic interactions in DySb has also been deduced previously from a mean-field analysis of elastic and magnetothermal data, and it was concluded that J'_{ij} is effectively positive [6, 7]. Although a positive J'_{ij} provides a plausible rationale for the first-order transition of DySb at T_N in zero field [7], it was shown more recently that the abruptness of this transition can be justified solely on the basis of magnetic symmetry [8].

*Work performed under the auspices of the US Energy Research and Development Administration.

†Supported in part by the National Science Foundation and the Office of Naval Research.

1044

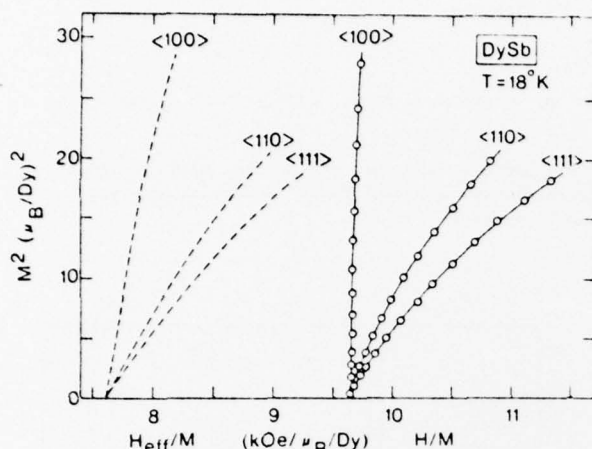


Fig. 2. Calculated (dashed) curves of M^2 vs. H_{eff}/M and experimental data of M^2 vs. H/M for DySb at 18 K with the effective field (H_{eff}), applied field (H), and magnetization (M) along various crystallographic directions.

In order to reveal explicitly any biquadratic coupling in DySb, we have followed a procedure recently used for the compound PrAg [9]. First, we had to determine the magnetization (M) vs. effective field (H_{eff}) behavior of DySb from its crystal-field states. The latter are presently available from interpolations between the neutron scattering results on various other isomorphous rare-earth antimonides [10]. We could thus establish quite reliably that the crystal-field coefficients for DySb are $A_4^0(r^4) = 60$ K and $A_6^0(r^6) = 2$ K, from which we deduced that relative to the lowest lying Γ_6 doublet the three Γ_8 quartets are at 8.8, 96.0 and 120.2 K, and the Γ_7 doublet is at 60.4 K [11]. From this crystal-field scheme, we calculated M vs. H_{eff} at various temperatures for H_{eff} along each of the principal crystallographic directions; the results for 18 K are presented as M^2 vs. H_{eff}/M in fig. 2. Also shown in this figure are our experimental magnetization results for DySb at 18 K in fields up to 56 kOe applied along the same three directions, which are plotted analogously as M^2 vs. H/M . These and similar experimental curves obtained at other temperatures within the paramagnetic regime were each compared against the corresponding calculated M^2 vs. H_{eff}/M isotherm; $(H_{\text{eff}} - H)/M$ was then evaluated at each experimental value of M^2 .

Our results are plotted as M^2 vs. $(H_{\text{eff}} - H)/M$ in fig. 3. They can be compared meaningfully

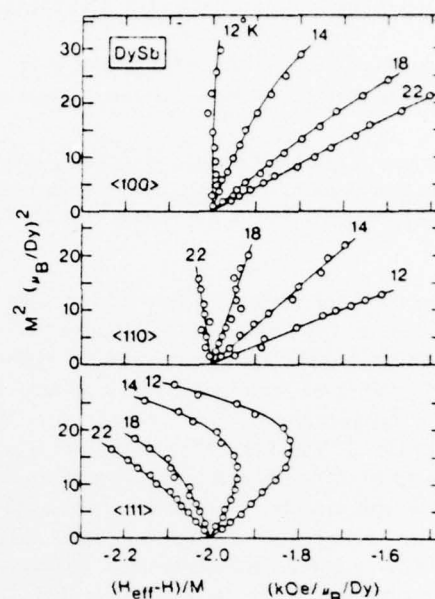


Fig. 3. M^2 vs. $(H_{\text{eff}} - H)/M$ for DySb at various temperatures (in K) for different directions of the effective field (H_{eff}), applied field (H), and magnetization (M).

with an expression for the total exchange field,

$$H_{\text{exch}} = H_{\text{eff}} - H = \lambda M + \lambda' M^3, \quad (2)$$

which has been derived [9] from spin hamiltonian (1) within a mean-field framework, where λ and λ' are proportional to the j -summations of J_{ij} and J'_{ij} , respectively, for the paramagnetic state. Thus, if λ and λ' were constant, M^2 vs. $(H_{\text{eff}} - H)/M$ would describe a straight line and, if λ' were zero, the line would be vertical. The pronounced deviations of the curves in fig. 3 from verticality can therefore be taken as evidence for substantial biquadratic interactions in DySb. Furthermore, these interactions vary significantly with temperature and with the direction (and, in some cases, the magnitude) of the magnetization. A detailed analysis of these results will be presented in a future report.

References

- [1] E. Bucher, R.J. Birgeneau, J.P. Maita, G.P. Felcher and T.O. Brun, Phys. Rev. Lett. 28 (1972) 746.
- [2] G.P. Felcher, T.O. Brun, R.J. Gambino and M. Kuznietz, Phys. Rev. B8 (1973) 260.
- [3] G. Busch and O. Vogt, J. Appl. Phys. 39 (1968) 1334.

- [4] T.O. Brun, G.H. Lander, F.W. Korty and J.S. Kouvel, AIP Conf. Proc. 24 (1974) 244.
- [5] P. Streit, G.E. Everett and A.W. Lawson, Phys. Lett. 50A (1974) 199.
- [6] T.J. Moran, R.L. Thomas, P.M. Levy and H.H. Chen, Phys. Rev. B7 (1973) 3238.
- [7] L.F. Uffer, P.M. Levy and H.H. Chen, AIP Conf. Proc. 10 (1973) 553.
- [8] P. Bak, S. Krinsky and D. Mukamel, Phys. Rev. Lett. 36 (1976) 52.
- [9] T.O. Brun, J.S. Kouvel and G.H. Lander, Phys. Rev. B13 (1976) 5007.
- [10] R.J. Birgeneau, E. Bucher, J.P. Maita, L. Passell and K.C. Turberfield, Phys. Rev. B8 (1973) 5345.
- [11] These crystal-field coefficients and energy levels for DySb differ somewhat from those deduced in ref. 1 from more limited spectroscopic information.

REPORT DOCUMENTATION PAGE		READ INSTRUCTIONS BEFORE COMPLETING FORM
1. REPORT NUMBER NR318-031-F	2. GOVT ACCESSION NO.	3. RECIPIENT'S CATALOG NUMBER
4. TITLE (and Subtitle) Magnetism in Transition-Group Alloys and Rare-Earth Compounds		5. TYPE OF REPORT & PERIOD COVERED Final Technical Report 1 Apr. 74 - 30 June 76
		6. PERFORMING ORG. REPORT NUMBER
7. AUTHOR(s) James S. Kouvel		8. CONTRACT OR GRANT NUMBER(s) N00014-75-C-0895 N00014-69-A-0090-0003
9. PERFORMING ORGANIZATION NAME AND ADDRESS Department of Physics University of Illinois at Chicago Circle Chicago, Illinois 60680		10. PROGRAM ELEMENT, PROJECT, TASK AREA & WORK UNIT NUMBERS NR318-031
11. CONTROLLING OFFICE NAME AND ADDRESS ONR Electronics and Solid State Sciences Program Arlington, Virginia 27217		12. REPORT DATE September 1977
14. MONITORING AGENCY NAME & ADDRESS (if different from Controlling Office) ONR Branch Office 536 S. Clark Street Chicago, Illinois 60605		13. NUMBER OF PAGES 53
		15. SECURITY CLASS. (of this report) Unclassified
		15a. DECLASSIFICATION/DOWNGRADING SCHEDULE
16. DISTRIBUTION STATEMENT (of this Report) Approved for public release; distribution unlimited.		
17. DISTRIBUTION STATEMENT (of the abstract entered in Block 20, if different from Report) -----		
18. SUPPLEMENTARY NOTES -----		
19. KEY WORDS (Continue on reverse side if necessary and identify by block number) ferromagnetism, mictomagnetism, exchange interactions, transition-group alloys, rare-earth compounds.		
20. ABSTRACT (Continue on reverse side if necessary and identify by block number) See following page.		

ABSTRACT

↓
Magnetization measurements were carried out in a study of local magnetic effects (magnetic clusters, paramagnons, etc.) in the transition-group alloy systems, Ni-Rh, Pd-Ni, and Fe-Cr, near their critical compositions or critical temperatures for ferromagnetic ordering. Similar measurements were made of the detailed magnetization processes associated with the micro-magnetic (spin-glass) ordering of Cu-Mn alloys. Also conducted was a magnetic and neutron diffraction investigation of high-order (biquadratic) exchange interactions in the rare-earth compounds, PrAg and DySb.

Unclassified

SECURITY CLASSIFICATION OF THIS PAGE(When Data Entered)

DISTRIBUTION LIST FOR ONR ELECTRONIC AND
SOLID STATE SCIENCES PROGRAM OFFICE

Director Advanced Research Projects Agency Attn: Technical Library 1400 Wilson Boulevard Arlington, Virginia 22209	1 copy
Office of Naval Research Electronics and Solid State Sciences Program Office (Code 427) 800 North Quincy Street Arlington, Virginia 22217	1 copy
Office of Naval Research Code 105 800 North Quincy Street Arlington, Virginia 22217	6 copies
Office of Naval Research Code 200 800 North Quincy Street Arlington, Virginia 22217	1 copy
Naval Research Laboratory Department of the Navy Attn: Code 2627 Washington, D. C. 20375	6 copies
Office of the Director of Defense Research and Engineering Information Office Library Branch The Pentagon Washington, D. C. 20301	1 copy
U. S. Army Research Office Box CM, Duke Station Durham, North Carolina 27706	1 copy
Defense Documentation Center Cameron Station Alexandria, Virginia 22314	12 copies
Director National Bureau of Standards Attn: Technical Library Washington, D. C. 20234	1 copy

Distribution List (Continued)

Office of Naval Research Branch Office 536 South Clark Street Chicago, Illinois 60605	2 copies
San Francisco Area Office Office of Naval Research 50 Fell Street San Francisco, California 94102	1 copy
Air Force Office of Scientific Research Department of the Air Force Washington, D. C. 20333	1 copy
Commanding Officer Office of Naval Research Branch Office 1030 East Green Street Pasadena, California 91101	1 copy
Commanding Officer Office of Naval Research Branch Office 495 Summer Street Boston, Massachusetts 02210	1 copy
Director U. S. Army Engineering Research and Development Laboratories Fort Belvoir, Virginia 22060 Attn: Technical Documents Center	1 copy
ODDR&E Advisory Group on Electron Devices 201 Varick Street New York, New York 10014	1 copy
New York Area Office Office of Naval Research 207 West 24th Street New York, New York 10011	1 copy
Air Force Weapons Laboratory Technical Library Kirtland Air Force Base Albuquerque, New Mexico 87117	1 copy
Air Force Avionics Laboratory Air Force Systems Command Technical Library Wright-Patterson Air Force Base Dayton, Ohio 45433	1 copy

Distribution List (Continued)

Air Force Cambridge Research Laboratory L. G. Hanscom Field Technical Library Cambridge, Massachusetts 02138	1 copy
Harry Diamond Laboratories Technical Library Connecticut Avenue at Van Ness, N. W. Washington, D. C. 20438	1 copy
Naval Air Development Center Attn: Technical Library Johnsville Warminster, Pennsylvania 18974	1 copy
Naval Weapons Center Technical Library (Code 753) China Lake, California 93555	1 copy
Naval Training Device Center Technical Library Orlando, Florida 22813	1 copy
Naval Research Laboratory Underwater Sound Reference Division Technical Library P. O. Box 8337 Orlando, Florida 32806	1 copy
Navy Underwater Sound Laboratory Technical Library Fort Trumbull New London, Connecticut 06320	1 copy
Commandant, Marine Corps Scientific Advisor (Code AX) Washington, D. C. 20380	1 copy
Naval Ordnance Station Technical Library Indian Head, Maryland 20640	1 copy
Naval Ship Engineering Center Philadelphia Division Technical Library Philadelphia, Pennsylvania 19112	1 copy

Distribution List (Continued)

Naval Postgraduate School Technical Library (Code 0212) Monterey, California 93940	1 copy
Naval Missile Center Technical Library (Code 5632.2) Point Mugu, California 93010	1 copy
Naval Ordnance Station Technical Library Louisville, Kentucky 40214	1 copy
Naval Oceanographic Office Technical Library (Code 1640) Suitland, Maryland 20390	1 copy
Naval Explosive Ordnance Disposal Facility Technical Library Indian Head, Maryland 20640	1 copy
Naval Electronics Laboratory Center Technical Library San Diego, California 92152	1 copy
Naval Undersea Warfare Center Technical Library 3202 East Foothill Boulevard Pasadena, California 91107	1 copy
Naval Weapons Laboratory Technical Library Dahlgren, Virginia 22448	1 copy
Naval Ship Research and Development Center Central Library (Code L42 and L43) Washington, D. C. 20007	1 copy
Naval Ordnance Laboratory White Oak Technical Library Silver Spring, Maryland 20910	1 copy
Naval Avionics Facility Technical Library Indianapolis, Indiana 46218	1 copy
Superintendent Materials Sciences Division Naval Research Laboratory Washington, D. C. 20375	1 copy